The anomalously-propagating South Kenya rift in the context of the North Tanzanian Divergence zone, East Africa

Bernard Le Gall, Remigius Gama, Alexander Koptev, Gilles Chazot, Nelson Boniface, Nicolas Loget, Mohamed Ahmed Daoud, Pascal Tarits, Matthieu Plasman, Sophie Hautot

The anomalously-propagating South Kenya rift in the context of the North Tanzanian Divergence zone, East Africa.

Bernard Le Gall[1*], Remigius Gama[2], Alexander Koptev[3], Gilles Chazot[1], Nelson Boniface[2], Nicolas Loget[4], Mohamed Ahmed Daoud[5], Pascal Tarits[1], Matthieu Plasman[6], Sophie Hautot[7]

[1]UMR/CNRS 6538 Géosciences Océan, Brest University, France

[2]Department of Geology, Dar es Salaam University, Tanzania

[3]Department of Geosciences, Tübingen university, Tübingen, Germany

[4]UMR 7193, ISTeP, Sorbonne university, Paris, France

[5]Centre d'Etudes et de Recherches de Djibouti, Djibouti

[6]Institut de Physique du Globe, Paris, France

[7]IMAGIR sarl, Brest, France

* corresponding author, blegall@univ-brest.fr

Abstract

The axial fault-bounded depression of the South Kenya rift (SKR) locally displays anomalously wide sectors resulting from the presence of one (or many) elevated and offset block(s) on the flanks of the main trough. Very little attention has been paid so far to the nature of the driving mechanisms responsible for these atypical rift patterns. New insights are supplied by the Natron-Ol Doinyo Ogol rift segment at the southern extremity of the SKR, immediately north of the North Tanzanian Divergence (NTD). On the basis of interpreted SRTM-30 satellite imagery and Digital Elevation Models, our work allows us: i) to depict the highly-segmented arrangement of the ~7 Ma-lasted SKR system, ii) to establish a two-stage kinematic rift model that emphasizes the role of an inherited transverse discontinuity on the arrest, as well as lateral jump and off-axis development of anomalously-propagating rift structures, iii) to define the relative contribution of border *vs* inner fault networks to the total extension, which is estimated at 7-6 km (11.6-9.2 %), and iv) to emphasize that inner faulting was not the dominant mode of strain accommodation during recent inward focussing of strain, and that no sharp transition exists from border fault- to intra-rift fault-dominated strain accommodation over time in the SKR immature rift system.

1. Introduction

The archetypal physiography of the reference East African Rift System (EARS, Fig. 1A) is a <100 km-wide fault-bounded depression composed of a succession of elongate volcano-sedimentary basins commonly displaying asymmetrical half-graben geometry (Rosendahl, 1987; Morley, 1988)

and along-strike segmentation (Corti, 2008; Keir et al., 2015). However, anomalously wide structural patterns locally express by offset and paired half-grabens as those present along the eastern magma-rich Kenya rift, in the Turkana and Baringo/Bogoria areas (Ebinger et al., 2000; Hautot et al., 2000), as well as in the Natron-Ol Doinyo Ogol sector further south (Figs. 1A, B). The kinematic conditions that prevailed during the emplacement of these atypical structures have not been yet explicitly addressed. New insights are provided by the Natron-Ol Doinyo Ogol system in the framework of the South Kenya rift (SKR) and the three diverging rift arms (Eyasi, Manyara and Pangani) forming the 200 km-wide North Tanzanian Divergence (NTD) further south (Figs. 1B, C) (Dawson, 1992). The influence of Archaean basement discontinuities on rift trajectory in the NTD *sensu stricto* has been previously advocated by Ebinger et al. (1997) and Le Gall et al. (2008), but there is a lack of wider-scale models relevant to the entire SKR-NDT rift system. The present study aims to propose a kinematic rift model using data from interpreted 30 m-resolution Shuttle Radar Topography Mission satellite (SRTM) imagery, focused on the Magadi-Natron axial trough and the poorly-investigated Ol Doinyo Ogol block (OOB), and locally constrained by field observations. Compiling surface geology, published volcanic age dataset and erosional features of the rift-bounding fault pattern allows for: i) depicting the complete morphostructural arrangement of the highly segmented SKR pattern, ii) proposing a two-stage kinematic model for the 7 Ma-lasted SKR-NTD system, iii) discussing the role of inherited discontinuities on rift kinematics, iv) for specifying the spatio-temporal distribution of extension in the SKR segmented pattern, and v) quantifying the respective contribution of both inner and border fault networks to the total extension.

2. Rift setting

At ~2°S, the linear half-graben architecture of the SKR (Chapman et al., 1978; King, 1978) gives way southwards to a more intricate rift configuration due to the presence of the 30 x 70 km losange-shaped OOB offset block, which is west of the Natron axial depression (Fig. 2). The corresponding rift-bounding fault-scarp network comprises, from N to S: the Nguruman, Sonjo, and Ol Doinyo Ogol (OOF) faults, all in an outer position to the west, and the innermost Sambu and Natron faults in the southern prolongation of the Nguruman fault. At the same latitude (2°S), the continuity of the eastern margin is disrupted by a 100 km-long and 30 km-wide triangle-shaped basement structure, the so-called Engare salient that causes the narrowing of the Natron trough (<40 km-wide), accordingly. At ~2°45'S, the trend of the Natron rift axis swings southwards into the NW/SE-oriented Engaruka depression before abutting against the Essimingor-Tarosero volcanic lineament (Figs. 1B, C). The latter is part of a series of transverse volcanic chains that also include the NE/SW Crater Highlands to the west and the EW-trending Tarosero-Kilimanjaro volcanic axis between the SKR magmatic rift and the mostly amagmatic NTD to the south (Figs. 1B, C) (Dawson,

1992; Le Gall et al., 2008; Isola et al., 2014). Rifting in the 200 km-wide NTD is achieved along three discrete diverging rift arms that are from W to E (Figs. 1B, C): i) the 150 km-long and SE-facing Eyasi half-graben basin, oriented NE/SW at a high angle to the Archaean-Proterozoic boundary, and filled with <3.5 km-thick sedimentary sequences (Ebinger et al., 1997); ii) the submeridian and <1.4 km-deep Manyara easterly-facing half-graben in the southern prolongation of the Natron axis (Ebinger et al., 1997), which continues southwards *via* a transverse network of seismically active faults (Macheyeki et al., 2008) into reactivated Karoo-age normal faults bounding the Kilombero valley (Le Gall et al., 2004); and iii) the Pangani basement ridge, south of the Kilimanjaro volcano, is composed of three right-stepping en echelon uplifted segments, possibly following an inherited NW/SE-oriented (ASWA-type) Proterozoic trend (Le Gall et al., 2008) that extend offshore into the Indian ocean along the Davie Ridge (Fig. 1A) (O'Donnell et al., 2013; Mulibo & Nyblade, 2016).

The SKR-NTD rift system developed in a highly heterogeneous basement comprised of the Tanzanian and Masai cratonic blocks overlain to the east by Proterozoic thrust-nappes displaced to the west during the collision-related East African orogeny at ~620 Ma (Figs. 1B, C) (Mosley, 1993; Moller et al., 2000). The Proterozoic frontal thrust pattern roots eastwards along a thrust-ramp likely guided at depth by the craton edge, 100-200 km east of its exposed boundary in the Mbulu plateau (Shackleton, 1993; Fritz et al., 2009). The Tanzanian craton itself is composed of smaller continental blocks amalgamated along NE/SW-oriented suture zones (Fletcher et al., 2018). Most of the basement uplifted plateaus bounding the SKR-NTD rift are composed of metamorphic rocks that display shallowly-dipping foliations, further affected by later map-scale folds (Figs. 1B, C) (Baker, 1958; Thomas et al., 2016). The crustal rift pattern is dominated by a marked crustal thinning from 40 km beneath the basement uplifted flanks to 35 km beneath the rift axis with the shallowest Moho depth in the Magadi trough to the north (Birt et al., 1997; Ritsema et al., 1998; Thybo et al., 2000; Sippel et al; 2017; Plasman et al., 2017; Tiberi et al., 2019). Receiver function modelling reveals that NE/SW-oriented oblique zones of lithospheric thinning occur at greater depths beneath the rift axis from the Crater Highlands to the Magadi trough (Plasman et al., 2017). A similarly-oriented, but shallower network of seismically-active faults is evidenced in the Gelai upper crust, i.e. the Naibor Saito earthquake swarm of Weinstein et al. (2017), as well as in the Manyara area further south (Albaric et al., 2010). These transverse rift trends are oblique to the EW extension determined from stress tensors (Ibs-von Seth et al., 2001; Delvaux & Barth, 2010; Albaric et al., 2014), geodetic records (Saria et al., 2014), and earthquake focal mechanism analyses (Albaric et al., 2014). Their origin as either inherited features (Albaric et al., 2010) or due to local stress rotations (Weinstein et al., 2017) is still debatable. Earthquake focal depths in the range 20-40 km reflect the relatively strong and mafic rheology of the lower crust (Albaric et al., 2009) and the importance of high fluid pressures related to magmatic chambers (Muirhead et al., 2016; Weinstein et al., 2017).

The general southerly younging of tectono-magmatic events along the ~7 Ma-lasted SKR system (Le Gall et al., 2008; Mana et al., 2015) is disturbed by anomalous age patterns in the southern transverse volcanic chains. There, magmatism migrated either to the NE (Lemagrut-Embagai and Essimingor-Tarosero lineaments), or to the E (Tarosero-Kilimanjaro chain) from discrete nucleation sites (Nonnotte et al., 2008; Mana et al., 2015). The tectono-magmatic evolution of the SKR-NTD system is usually subdivided into two successive stages. The early stage (7-1.3 Ma) is dominated by two various styles of magmatism with specific spatial distributions (Fig. 2). Extensive flood-type lavas initiated to the North with the emplacement of the ~7 Ma-old Longitoto trachytes in the nascent Magadi-OOB-Natron rift depression as far south as 2°S. These rocks are currently preserved as narrow faulted strips on top of uplifted basement relief bounded by the Nguruman fault system along the Magadi trough (Baker, 1958). The Narok basement bounding plateau to the east is capped by nearly coeval, but unfaulted lavas. These initial flood lavas were later punctuated by a series of axial shield volcanoes comprising the Olorgesailie (2.7-1.7 Ma), Lenderut and Shombole (2.0 Ma) edifices (Baker, 1958; Baker et al., 1971; Fairhead et al., 1972; Crossley, 1979; Birt et al., 1997). Magmatism initiated later in the OOB offset block with the effusion of 3.5 Ma-old flood-type basalts (Fig. 3A) (Muirhead et al., 2016), referred to here as the Salei series in order to avoid any confusion with the <3.5 Ma-old Ol Doinyo Sambu lavas (Isaac & Curtis, 1974). In the time-range 1.7-1.3 Ma, terrigeneous/lacustrine deposits and interlayered lavas of the Peninj series were deposited in the Sanjan faulted sub-basin, in the eastern part of the OOB (Isaac & Curtis, 1974; Manega, 1993; Forster et al., 1997). Further south, off-axis magmatic intrusions occurred as early as 5 Ma in the oblique Crater Highlands range in association with lavas younging gradually to the NE (Bagdasaryan et al., 1973; McIntyre et al., 1974; Manega, 1993; Foster et al., 1997).

During the later stage (1.3 Ma-Present), a second episode of flood lava resulted in the effusion of the 1.3-0.9 Ma-old Magadi trachytes (c. 400 m-thick) over the still subsiding Magadi-Natron floor (Isaac & Curtis, 1974; Muirhead et al., 2016), concomitantly to major fault activity along the E/Nguruman-Sambu-Natron border fault system (McIntyre et al., 1974). During the late rifting stage, a major change expressed by a dense swarm of rift-parallel normal faults disrupting the Magadi trachyte axial floor (Baker et al., 1988). Inward migration of strain towards the rift axis is attributed to magma and related volatile release (Muirhead et al., 2016; Lee et al., 2017). More locally, the influence of transverse basement structures on the geometry and kinematics of these young inner rift structures is argued from the Kordjya fault zone in the Magadi trough (Le Turdu et al., 1999; Muirhead & Kattenhorn, 2018). Active strain is still partly accommodated by slip along the Natron border fault (Kervyn et al., 2008; Sherrod et al., 2013; Muirhead et al., 2016) and by the combined effect of dike intrusions and normal fault slip in the rift axis as documented during the 2007 Lengai-Gelai seismo-tectonic crisis (Calais et al., 2008; Baer et al., 2008; Albaric et al., 2010). From a recent quantitative

analysis of strain, Muirhead et al. (2016) emphasized that: i) the relative contribution of border faults (*versus* intra-rift faults) in the regional extension is greater in the Natron segment (c. 70%) than in the Magadi segment (c. 30%), and ii) most of intra-rift extension in the Natron segment resulted from the flexure of the downthrown hangingwall (Natron trough) during border fault activity. Since these authors did not integrate the OOB offset block in their structural analysis, their results are thought not to be representative of the entire SKR system and are thus fully discussed in the present study.

3. Methodology

The SKR-NTD rift system under study extends at 1°30'-3°30' and 35°30'-37°E (Figs. 1B, C). It does not include the discrete Pangani rift arm on the eastern side of the NTD (readers can refer to Le Gall et al. (2008) for details). The morphostructural analysis of the SKR is primarily based on the interpretation of SRTM-30 m imagery (SRTM V3.1,1 arcsec., Universal Transverse Mercator projection following Geodetic System WGS84) with lateral and vertical resolutions of 30 m and 8 m, respectively. The qualitative and quantitative analyses of both the border and intra-rift fault networks extracted from this dataset help us to define the structural style of extension in the Magadi-Natron trough. The main structural attributes of individual faults (length, maximum displacement) are estimated, based on the above-mentioned resolutions of the SRTM dataset. As most fault map traces are tortuous and highly segmented, fault lengths have been measured as tip-to-tip linear distances, including the cumulative lengths of overlapping segments (Fig. 4A) (Vétel et al., 2005). The height of exposed individual fault scarps is considered as a proxy for minimum vertical displacement (throw) (Fig. 4B), being aware that: i) the foot of fault planes is usually covered by scree deposits, as observed in the field along the OOF and Natron-Sambu faults (Fig. 3D), ii) the early history of faults might not have been recorded by their visible scarps, and iii) the top-most part of uplifted footwall blocks might have been partly removed by erosion (Fig. 3C). In the latter case, the maximum height of the incised fault scarps has been measured by using their envelop surface as a topographic marker. Throw estimates along master rift-bounding faults have been calculated from three complementary datasets supplied by: i) geophysically-recorded basement depths, ii) thicknesses of presumably syntectonic hangingwall sequences, and iii) fault scarp elevations. The latter have been corrected by adding the estimated height of material removed by erosion on top of the uplifted footwall blocks. For individual faults (both inner and border structures), throw measurements have been regularly performed on a series of short topographic profiles, orthogonal to the fault trace and with a constant spacing depending on the total length of the fault. The maximum throw value (T_{max}) obtained for each fault has been converted to maximum displacement (D_{max}) and extension (h = heave) by assuming an optimal 60° dip for the fault plane (in agreement

with previous works elsewhere in the EAR, e.g. Ebinger et al., 1989; Wheeler & Rosendahl, 1994) and by using the classical trigonometric equations:

$$h = T/\tan 60°,\ D = T/\sin 60°$$ (Fig. 4B)

Fault displacement profiles (x 140) have been used: i) to constrain mechanisms of inner fault propagation in the Magadi-Natron trough, and ii) to test whether the Engare intra-rift salient may have acted as a mechanical barrier to rift/fault propagation.

Master and inner fault-related extensions have been summed along 12 regularly-spaced (10 km) cross-sections in order to document any lateral variations of extension along a 110 km-long, rift-parallel transect (Figs. 2A, 5A). The eventual strike-slip component of faults in the SKR is assumed to be minor given the general submeridian orientation of the entire fault population which is nearly orthogonal to the EW direction of extension. Because our quantitative fault analysis is primarily focused on throw (extension) measurements, only 3D-dataset provided by SRTM-30 imagery and corresponding DEM's have been considered in the present work. For that reason, better resolution 2D-imagery data (aerial photos) that could have provided more accurate length values has not been used here, resulting in undersampling of minor fault populations beyond the SRTM-30 resolution. The latter are assumed not to contribute a significant amount to extension with respect to the km-scale values attributed to border faults from geophysically-based basement depths (see below). Therefore, biases in throw and length measurements are insignificant and do not degrade our results, considered as acceptable data for comparative purposes. Field investigations carried out in the OOB offset basin aim: i) to document erosional features along its bounding fault system and ii) to sample sedimentary infill series drawn as small inliers on published geological maps (Fig. 2B).

4. Results

The morphostructural analysis of the SKR concerns not only the relatively young Magadi-Natron rift valley, but also more eroded and presumably older rift structures (OOB, W/Nguruman fault scarp) that might have recorded early rift stages (Fig. 2) and must be thus fully considered, more especially in terms of bulk extension estimates.

4.1. The SKR rift morphology

4.1.1. The western rift-bounding fault network

The Magadi-Natron/OOB downthrown domain is bounded to the west by a highly-segmented master fault network (Fig. 2). To the north, it comprises of the >60 km-long Nguruman fault network, composed of a >10 km-spaced double-fault system and associated uplifted footwall blocks (Fig. 5). The narrow and <1800 m-high inner block is capped by the 7 Ma-old Longitoto trachytes that exceed 400 m in thickness to the south (Fig. 2D1) (Baker, 1958). These lavas are cut to the east by the

E/Nguruman fault-scarp that limits the Magadi trough with elevations in the range 1000-1800 m. At its southern tip line, the E/Nguruman fault splits into two closely-spaced and steep faults (Fig. 5). The outer and higher footwall block is exclusively composed of highly-folded metamorphic (Proterozoic) rocks in the >2400 m-high Loita plateau. The sharp truncation of map-scale basement folds by the three right-stepping and overlapping fault segments forming the W/Nguruman fault-scarp indicates that Proterozoic basement ductile fabrics did not exert any structural control on the Magadi bounding fault network (Fig. 5A). The deep incision of the W/Nguruman basement footwall block, as well as the eroded profile of its fault-scarp, typically evoke early rift structures (Figs. 2D1, 5B) that likely developed synchronously to the effusion of the 7 Ma-old Longitoto lavas in the proto-Magadi half-graben (Crossley, 1979; Baker et al., 1988). The less incised topography of these lavas in the footwall of the E/Nguruman fault suggests younger uplift in a more inner position, presumably during the emplacement of the 1.3-0.9 Ma Magadi trachyte series in the Magadi hangingwall trough (Baker, 1958; Muirhead et al., 2016). In agreement with Baker (1958), we come to the conclusion that the twinned Nguruman master fault scarps (W/ and E/) initiated diachronously during a multistage faulting process, concomitantly to two successive lava flood episodes in the time-range 7-0.9 Ma.

At 1°53'S, the Nguruman border fault system splits into two diverging faults (Figs. 2, 5). Its overlapping zone with the colinear Sambu fault is a 20 x 10 km relay zone occupied by a 400 m-thick succession of Longitoto trachytes. Further south, the 40 km-long and >1300 m-high Sambu fault-scarp cuts through the 3.5-1.9 Ma-old Sambu volcano (Isaac & Curtis, 1974; Manega, 1993; Muirhead et al., 2016) and underlying Proterozoic basement terrains. The Sambu fault connects southwards *via* a 20 km-long transfer fault into the >60 km-long and 6-700 m-high seismically active Natron fault-scarp (Sherrod et al., 2013; Muirhead et al., 2016), the footwall of which is composed of the Peninj sediment/lava succession and the underlying 3.5 Ma-old Salei basalts (Muirhead et al., 2016) that floor most parts of the OOB offset block to the west (Fig. 3D). Its immediate hangingwall is occupied by lake Natron and recent sediments overlying the Magadi trachytes series at depth.

At 1°53'S', the Nguruman fault system also connects laterally westwards into the N60°-oriented and 40 x 25 km Sonjo transfer zone that comprises of a dense network of closely-spaced normal faults (x 5-6), facing dominantly to the SE (Figs. 2, 5). They bound narrow (2-3 km-wide) faulted blocks stepping down gradually towards the OOB volcanic floor (Fig. 5C). Individual fault scarps, >700 m-high, limit deeply incised basement blocks, probably uplifted during an early faulting event.

The Sonjo transfer zone in turn links to the SW with the submeridian and segmented OOF fault-scarp that sharply cuts through highly-folded Proterozoic footwall rocks in the Loliondo plateau. These eroded basement flanks, as high as 2300 m to the north (Fig. 3C), topographically decrease southwards down to 1700 m towards a tip point close to the Crater Highlands (Figs. 2A, B). The OOB hangingwall block is composed of the Salei basalts, exposed as a >200 m-thick volcanic pile in the

Sanjan fault scarp, to the east (Figs. 2B, D2). Assuming that the 3.5 Ma-old Salei basalts were erupted synchronously to the OOF activity suggests that the entire offset bounding fault network propagated diachronously southwards in the time-range 7-3.5 Ma.

Baker's (1958) concept about the key-role of the Nguruman rift-bounding fault is confirmed by geophysical records showing crustal thickness variations (from 35 to 29 km eastwards) beneath its exposed scarp (Birt et al., 1997; Plasman et al., 2017) and ~3km of downthrow of the Magadi hangingwall basin (Ebinger et al., 1997). The lack of appropriate geophysical data in the OOB prevents any accurate estimates of basement depth and cumulative displacement along the OOF border fault. Therefore, the modest throw value estimated above from surface geology is probably underestimated compared to the crustal nature of the fault suggested by geophysical data. Indeed, magnetotelluric profiles show two contrasting upper crustal blocks on both sides of the extrapolated trace of the OOF (Fig. 2A) (Plasman et al., 2019). The resistive block to the west corresponds to the unrifted basement crust close to the western craton edge, whereas the more conductive upper crust to the east correlates with the OOB-Crater Highlands-Natron magmatic rifted domain. The crustal nature of the OOF master fault is further confirmed by receiver function modelling that revealed the step-like geometry of the Moho which shallows eastwards from 40 km beneath the basement uplift block up to 35-37 km beneath the Salei plain in the OOB hangingwall block (Plasman et al., 2017). These results emphasize the prominent role of the OOF structure and therefore have major implications on the hierarchy of the rift-bounding fault network in the SKR system.

4.1.2. The intra-rift structural pattern

The OOB offset block

On the geological map in Fig. 2B, the OOB offset block is subdivided into two submeridian compartments on both sides of the 30 km-long Sanjan normal fault. The latter is capped and post-dated to the south by lavas of the 3.5-1.3 Ma-old Mosonik volcano (Isaac & Curtis, 1974; Manega, 1993; Foster et al., 1997; Sherrod et al., 2013). In the immediate hangingwall of the OOF, the 25 x 80 km Salei plain is floored by the flat-lying Salei basalts that recorded no extension since 3.5 Ma, provided that any tilted-fault block was not later erased by erosion. Evidence for younger extension are observed further east along the Sanjan and Natron extensional faults that both limit the 1.7-1.3 Ma-old Peninj lacustrine/volcanic series (Fig. 2D2) (Isaac, 1965; Manega, 1993; McHenry et al., 2011).

Structural style in the Magadi-Natron rift valley

The morphostructural asymmetry of the Magadi-Natron trough typically characterizes an easterly-facing half-graben (Baker, 1958) which narrows gradually southwards from 70 to 40 km at the latitude of the Engare salient (Figs. 2B, D). Its along-strike segmentation into the Magadi (N) and

Natron (S) segments is variously expressed by: i) the decreasing elevation of the bounding footwall relief from ~2400 m (Nguruman) down to ~1300 m (Sambu-Natron) (Fig. 5), ii) the step-like topographic profile of the inner floor that dips southwards (from 1200 m down to 600 m) over 50 km (Magadi), and then shallows over 40 km (Natron), before rising up abruptly *via* a major fault-like step close to the Gelai volcano, into the 950 m-high Manyara floor (Fig. 2C), and iii) the southerly shallowing of basement depth from 3 km to 1.6 km along the Magadi-Natron basinal transect (Birt et al., 1997; Ebinger et al., 1997; Roecker et al., 2017).

The most complete structural cross-section of the Magadi-Natron half-graben occurs north of the Kordjya transverse fault (Figs. 2B, D1, 5B). It exhibits three distinct domains that are from W to E; i) two westerly-tilted fault blocks, 10 km-wide each, bounded by two normal faults synthetic to the master fault and with maximum displacement of ~300 m. Their southern extent is masked in the topographically subdued lake Natron area. ii) A 15 km-wide axial fault belt, dissected by a closely-spaced (<1 km) network of both synthetic/antithetic normal faults, extends as far south as the Gelai volcano. The resulting horst/graben pattern is dominated by two >40 km-long asymmetrical grabens that both narrow southwards (Fig. 6A), one of them hosting the Magadi lake to the NW. Most of the axial fault lengths are in the range of 2-50 km (Figs. 6B, C). Their zig-zag map-traces involve numerous fault segments (<7-8 in average), identified following Vétel et al. (2005), with lengths ranging from <1 km to 30 km. Various types of segment linkages are identified as collinear synthetic, approaching and synthetic overlapping patterns (Fig. 6A1), according to the classification of Morley (1999). iii) The >30 km-wide flexural margin to the east is a weakly faulted monocline, dipping regularly westwards from 1300 m up to a 2000 m-high basement bounding relief locally overlain by the Narok lava plateau as far south as 1°55'S (Fig. 2). This flexural margin surface is cut by a limited number of minor extensional faults displaying dips antithetic to the western master fault. Further south at 2°S the half-graben margin corresponds to a transverse structure, evoked earlier as the Engare basement salient (Fig. 5A). The latter forms a >2000 m-high, highly eroded transverse relief arranged into oblique and asymmetric tilted fault-blocks. Their SE-dipping envelop surfaces are cut by a network of N60°E normal faults, <5 km in length, facing consistently inwards.

4.2. Intra-rift fault analysis

4.2.1. Inner fault distribution in the Magadi-Natron trough

In the SKR under study, intra-rift faults are restricted to the Magadi-Natron volcanic inner floor. For simplicity, the latter is here considered to be uniformly composed of the Magadi trachyte series, since its subdivision into local volcanic formations (Muirhead et al., 2016) does not appear to supply any further insights into the first-order spatio-temporal development of inner strain. In the same way, the thin sediments that locally overlie the volcanic floor (Baker, 1958) are assumed to not

have recorded any significant fault-related strain history. The inner fault array is heterogeneously distributed over the volcanic axial floor. Fault density is maximum in the ~15 km-wide axial belt extending continuously from the Magadi lake (N) to the Gelai volcano (S). The flexural hinge zone to the east is much less faulted with a 15 km-wide monoclinal volcanic surface that dips regularly westwards (Figs. 2, 5). The relatively high density of inner faults results in a spacing mode (maximum frequency) of < 3 km on the 12 cross-sections in Fig. 2A.

4.2.2. Displacement/length profiles

Insights into the propagation and slip history of the inner fault population in the Magadi-Natron axial trough provided by analyzing the displacement/length values of the 140 individual structures extracted from the SRTM 30 imagery (Fig. 5A, details in Section S1 in Supplemental Materials). Fault length distribution ranges over three orders of magnitude from 2 km up to >50 km with a peak value in the class 5-10 km (Fig. 6B). When plotted on the log-log diagram in Fig. 6C, their D_{max}/L ratios define a field that fits within the linear distribution established from published data (Kim & Sanderson, 2005). Most of inner fault displacement profiles (~85%) display asymmetrical shapes that typically characterize restricted fault growth (Pollard & Segall, 1987; Dawers et al., 1993). This process is generally attributed either to interactions with confining features (Peacock, 1991; Burgmann et al., 1994; Nicol et al., 1996) or to the mechanical effect of stronger material acting as barriers to fault propagation (Aki, 1979). The second hypothesis can be tested about the restricted faults (~20) located north of the Engare basement salient (Fig. 5A). Their consistent northerly-restricted tips, genetically unrelated to any mechanical barrier to the south, allow us to exclude the second hypothesis. It is thus suggested that inhibition of inner fault tip propagation in the entire Magadi-Natron trough resulted from strong interactions in a closely-spaced fault network, as commonly documented in fault systems elsewhere (Dawers & Anders, 1995). The only conceivable structural impact of the Engare salient on the SKR rift pattern is to have provoked the gradual narrowing of its axial trough over a >30 km-long rift-parallel section and thus to have possibly caused a deficit of extension accordingly.

4.3. Extension estimates

With regards to previous structural works, one specific aspect of our study is to consider, not only the Magadi-Natron axial trough (Muirhead et al., 2016), but also the OOB offset block. That allows a more accurate and unbiased quantitative estimate of extension in the entire SKR system.
Extension calculations have been made with the aim of quantifying the respective contribution of border and intra-rift fault networks in the total extension recorded by the SKR system.

Before interpreting the extension results, it is necessary to define the temporal development of each fault pattern with respect to the multi-stage rift scenario envisaged above. Early extension (in the time-range 7-1.3 Ma) is assumed to have been exclusively accommodated by slip along the outermost W/Nguruman-OOF offset bounding fault network, whilst younger extension was achieved by the combined and multistage activity of: i) the innermost and linear E/Nguruman-Sambu-Natron border fault system, synchronously to the 1.3-0.9 Ma Magadi trachyte, and ii) the axial rift fault swarm post-dating the youngest (0.9 Ma) sequences of these lavas in the Magadi-Natron trough. Assuming the twinned nature of the Nguruman bounding scarp (W/ and E/ faults), in agreement with Baker (1958), leads us to emphasize its prominent role, in contrast with Muirhead et al. (2016) who only considered the innermost (E/Nguruman) scarp.

The total throw/extension values are calculated along 12 E-W cross-sections ($A_{1\text{-}12}$) that span the entire width of the SKR system with a constant spacing of 10 km (Figs. 2A, 5). Inner fault-related extension has been obtained by summing individual fault extension along each cross-section. As mentioned above, these are minimum estimates that might not have recorded earlier (not visible) slip history. According to Muirhead et al. (2016), the intra-rift fault network in the Magadi-Natron axial trough originated from the combined effect of regional (far-field) stress and more local hangingwall flexuring along its border fault system. Flexure-related extension nearly amounts 100% in the Magadi trough and thus corresponds to the values calculated below. In contrast, it is estimated at 10% in the Natron trough (Muirhead et al. (2016) and is considered a negligible value. Extension in the 20 km-wide immediate hangingwall of the border fault system has been accurately measured (~195 m) along only two continuously exposed cross-sections to the north ($A_{1\text{-}2}$). This value has then been extrapolated southwards to the Natron subdued area. Border fault-related extension has been calculated by summing three types of data which are (see Section 3, Fig. 7): i) the thickness of the syntectonic volcanics, evaluated at 400 m for the 7 Ma-old Longitoto trachytes currently exposed in the W/Nguruman footwall block and inferred to underlie the Magadi trachyte inner floor as far south as 2°S; 400 m for the 1.3-0.9 Ma Magadi trachytes (Baker, 1958) in the hangingwall of the younger E/Nguruman-Natron fault; and >400 m for the 3.5 Ma Salei basalts in the hangingwall of the OOF. ii) Geophysically-derived basement depths in the Magadi-Natron trough (Birt et al., 1997; Ebinger et al., 1997) suggest that a >3 km- and >1.5 km-thick buried synrift package underlies the Magadi and Natron axial volcanics, respectively, in relation with the earliest activity of the W/Nguruman fault. iii) Topographic elevations of the bounding fault scarps have been corrected by adding the estimated height of the eroded material. These corrections are based on correlations with thermo-chronology results (apatite, U-Th/He methods) obtained on the long-term denudation history of elevated flanks in the South Ethiopia (Pik et al., 2008; Baliesteri et al., 2016), North Kenya (Boone et al., 2018), and Rukwa-Malawi rifts (Van der Beek et al., 1998). Values in the range 100-220 $m.Myr^{-1}$ are confidently

applied to the SKR rift-bounding fault network, assuming striking similarities about the age of the onset of faulting (< 10's Ma), the magnitude of fault displacement, the lithology of the footwall material, and the climatic framework. Among the three complementary types of data above, both basement depths and lava thicknesses are constant. Although these data have been published without any error bars, they are assumed not to degrade our results since they are repeated on all sections and are thus considered as acceptable data for comparative purposes. Uncertainties only concern the applied erosion ranges and the estimated elevations of the corresponding fault scarp. Total throw/extension in the Magadi and Natron rift segments have been calculated for each cross-section $A_{1\text{-}4}$ and $A_{8\text{-}12}$, respectively. The contribution of the Sonjo transfer faults (sections $A_{5\text{-}7}$) has not been taken into account because of their obliquity to the EW direction of regional extension. Cumulative throw/extension values are represented in the diagrams in Figs. 8 by mid-points with error bars relative to the lower/upper limits of the corresponding denudation rates (Table 1). Error bars are maximum about the long-lasted Magadi border fault system. The results are represented as either finite extension values in km (W_1 - W_0), where W_0 and W_1 are the initial and final width of the rifted domain, respectively, or as the ratio in % such as

$e = (W_1 – W_0) / W_0$ (Table 1).

The prominent contribution of the two geophysically-derived basement depths in the cumulative throw estimates results in the dramatic step-like geometry of most extension profiles at the Magadi-Natron transition zone (Fig. 8).

Extension profiles in Fig. 8A concern each specific fault pattern in the entire SKR system: i) Early border fault-related extension (blue curve) decreases abruptly southwards at the Magadi-OOB/Natron transition zone (section A_5 in Fig. 2A) from ~4000 m (W/Nguruman) down to ~1000 m (OOF) *via* the Sonjo transfer zone. This sharp decrease (~3000 m) of early extension is probably exaggerated as early displacement/throw along the poorly-constrained OOF border fault might have been greater than the 500-1000 m estimated from surface geology. Inversely, younger extension (yellow curve) rises southwards at A_5 from <1000 m (E/Nguruman) up to ~1800 m (Sambu-Natron). The step-like geometry of extension profiles clearly illustrates the along-strike segmentation of the SKR rift pattern and further indicates that this process initiated at an early rifting stage and then persisted throughout time. ii) In contrast, inner fault-related extension values decrease smoothly southwards on the 110 km-long transect from ~1100 m (A_2) down to ~450 m (A_{12}) without any break at the Magadi-Natron transition. iii) No significant drop in inner extension is observed at the latitude of the Engare salient (A_7-A_{10}). iv) During the late rifting stage (yellow curves), the contribution of the bounding fault pattern relative to the inner fault pattern increases markedly southwards from ~50% in the Magadi basin (E/Nguruman fault), where the two curves nearly coincide in the range 1000-800 m, up to 80-75% in the Natron basin (Sambu-Natron fault).

The diagram in Fig. 8B concerns the total extension experienced by the multistage Magadi-Natron half-graben during its 7 Ma-lasted rift development. The cumulative extension recorded along the entire border fault pattern (green curve) is still highly segmented at the Magadi-Natron transition. The dramatic drop from 6700-5500 m (W/ and E/Nguruman) to 2400-1800 m (Sambu-Natron) mostly results from the oldest and prominent W/Nguruman fault.

The diagrams in Figs. 8C, D represent the cumulative extension in both the Magadi-Natron (8C) and entire SKR rift systems (8D): i) The total extension (border fault- and inner fault-related) drops abruptly southwards at the A_5-A_6 transition zone from the Magadi (7200-6200 m, 11.6-9.2 %) to either the Natron segment (3100-2700 m, 5.5-4.7 %) or to the Natron/OOB system (4400-3700 m, 6.0-3.9 %), with a significant contribution of the OOB block (2.4-0.8 %), being aware that these values are probably underestimated for reasons mentioned above.

4.4. Evidence for a first-order inherited transverse discontinuity

The structural sketch map of the SKR-NTD rift system in Fig. 9 is compiled from SRTM-30 DEM features, surface geology (Baker, 1958) and, more importantly, the seismicity pattern of Weinstein et al. (2017). It clearly shows a prominent lineament extending over >200 km in a NE/SW direction, oblique to the rift axis, from the Engare salient to the Eyasi fault tip. The map-trace of the so-called Engare-Eyasi lineament is outlined by the alignment of various rift structures that are from NE to SW: i) the early normal fault network bounding the Engare transverse tilted fault blocks, ii) the 1 Ma-old Gelai volcanoe and the surrounding Naibor Soito earthquake swarm (Weinstein et al., 2017) that includes events related to the 2007 Lengai-Gelai seismo-tectonic crisis with nodal fault planes typical of NNE/SSW extensional structures (Calais et al., 2008; Baer et al., 2008; Albaric et al., 2010), iii) the fault-like morphological scarp that disrupts the inner floor at the Natron/Engaruka segment transition, iv) the prominent Crater Highlands magmatic range and its NE/SW-oriented eruptive centres that parallel seismically active faults (Weinstein et al., 2017), and v) the 150 km-long Eyasi fault-basin system that dies out in Archaean terranes, 70 km SW of the exposed craton-Proterozoic boundary. To the NE the Engare-Eyasi lineament gives way to a >200 km-long morphological feature bounding to the SE the Narok-Nairobi phonolitic plateau (Upper Miocene) and Pleistocene lavas of Mount Kenya (Inset in Fig. 9). In the study area the linear and composite map-trace of the Engare-Eyasi lineament *sensu stricto* is assumed not to be fortuitous and suggests its structural control by a steeply-dipping and basement-rooted discontinuity that is collinear with Archaean/Proterozoic fabrics in the Mbulu plateau to the SW (Fig. 9). The variety and contrasting ages of rift features along the inherited Engare-Eyasi discontinuity argue for its long-lived and multi-stage reactivation during Neogene-Present extension. Its upper crustal nature is indicated by the 5-15 km depth range of most epicentres in the Naibor Soito earthquake swarm of Weinstein et al. (2017) (Fig. 9).

5. Discussion. Implications about rift propagation

5.1. Space-timing distribution of strain in the SKR system

An innovative aspect of our work with regards to previous structural studies about the SKR rift system is to integrate poorly investigated structures, such as the W/Nguruman bounding fault, the OOB offset block and the Engare basement salient. This approach leads us: i) to depict the complete morphostructural configuration of the entire SKR system, ii) to elaborate a revised (two-stage) kinematic model for its 7 Ma-lasted development, and iii) to perform a quantitative analysis of extension that differs markedly from earlier studies (Muirhead et al., 2016).

5.1.1. A two-stage rift model

While uncertainties still exist about the exact timing of the onset of displacement along rift-bounding faults in the SKR system, their contrasting erosional profiles suggest a two-stage faulting history, tentatively calibrated by available age dataset of synrift volcanics (Fig. 10). Initial rifting in the time-range 7-1.3 Ma was primarily achieved through displacement along the W/Nguruman/OOF dextrally-offset boundary fault network that accommodated asymmetric subsidence in the nascent Magadi-Natron/OOB half-graben basin (Fig. 10B). Earlier development of the Magadi basin, prior to 7 Ma, is hypothetized from geophysically-derived basement depths (Birt et al., 1997; Ebinger et al., 1997) that suggest the existence of a >2 km-thick buried synrift package beneath the initial Lengitoto volcanics (Fig. 7). The inferred proto-Magadi synrift basin might correlate with basement-derived sedimentary deposits known to pre-date magmatic activity in Central (Kerio) and North Kenya (Turkana) rift segments (Chapman et al., 1978; Morley et al., 1992; Mugisha et al., 1997; Hautot et al., 2000). The discrete inliers of limestones overlying Proterozoic basement rocks at the foot of the OOF in the OOB offset basin (Figs. 2B, 3A) (Dundas & Awadalla, 1966) might represent equivalent, but younger, initial synrift sequences, depending on their pre- or post-Salei basalt position. The identification of stromatolith-like organisms in the limestones rather supports the second hypothesis, and suggests their origin as remnants of westerly-thinned basal lacustrine deposits (Peninj formation), initially overlapping the Salei basalt substratum to the west. Intra-formational brecciated facies enclosed in the limestones (Fig. 3B) could be genetically related to syn- to post-depositional hydrothermal events in the OOB offset basin at that stage.

As envisaged below, it cannot be excluded that at one stage of initial rifting the W/Nguruman fault propagated as far south as the Engare-Eyasi transverse lineament. Transfer of strain from the W/Nguruman to the OOF border fault was achieved *via* the Sonjo structure that differs from most transfer faults in the EARS in terms of map-dimensions (25 x 40 km) and dominantly extensional kinematics of its internal faults. Concomitantly, the Magadi and Natron/OOB segmented hangingwall

basins were the locus of diachronous flood-type magmatism younging southwards from 7 Ma (Lengitoto trachytes) to 3.5 Ma (Salei basalts), respectively. The flat-lying and apparently unfaulted geometry of the OOB basin floor attests that it did not experience any significant intra-rift deformation at this early stage, as similarly assumed about the proto-Magadi/Natron basin. It is thus argued that the bounding fault system was the chief contributor to bulk brittle strain during initial rifting in the SKR.

The general southerly propagation of early tectonic and magmatic rift structures in the time-period 7-1.3 Ma was disturbed, as early as 5 Ma, by the off-axis emplacement of magma in the discrete Crater Highlands range to the SW (Lenderut, Sadiman edifices).

Fundamental changes in the mechanisms of rifting occurred in the time-range 1.3 Ma-Present, and resulted in the easterly (inward) shift of strain *via* two prominent processes that partly overlapped over time. The earlier stage was dominated by the inward migration of border fault activity: i) from the W/ to E/Nguruman fault to the north, and ii) from the abandoned and now-extinct OOF towards the Sanjan intra-basin fault and then to the Sambu-Natron fault in the southern prolongation of the E/Nguruman fault. At this stage, the Magadi-Natron downthrown half-graben was filled up with the 1.3-0.9 Ma Magadi trachyte flood-type lavas. Later on (<0.9 Ma), the axial volcanic floor was disrupted by a dense swarm of minor intra-rift normal faults that accommodated for the first time part of the regional extension.

5.1.2. Border *vs* inner fault-related strain accommodation

This pivotal issue about the evolution from border to intra-rift fault development in the SKR system needs to address: i) the spatial variations of extension along both the border and inner fault networks, and ii) the relative contribution of the two fault systems to the total extension recorded by the Magadi-Natron axial trough on one hand, and by the entire SKR rift system (including the OOB offset block) on the other hand. Quantitative results about extension are synthetized in Fig. 11. These results demontrate that: i) border fault activity is a greater contributor to extension in the Magadi segment (89-82 % along the multi-stage W/ and E/Nguruman fault) than in the Natron segment (85-77 % along the Natron fault), ii) intra-rift extension gradually decreases southwards from the Magadi to the Natron segment in agreement with the corresponding extension rates of Muirhead et al. (2016), iii) the relative contribution of the Natron fault system (5.5-4.8 %, border and intra-rift structures) to the total extension recorded by the southernmost SKR segment is minimized with respect to the results of Muirhead et al. (2016) because part of extension was accommodated by the OOF border fault (2.4-0.8 %).

Upper crustal extension achieved by brittle strain in the SKR is maximal (7200-6200 m, 11.6-9.2 %) in the Magadi northern segment, and it is compatible with the magnitude of crustal stretching (35 - 29

= 6 km, ß-factor of 1.2) deduced from geophysical data (Birt et al., 1997; Ebinger et al., 1997). It is thus suggested, at first approximation, that magma-assisted extension through dyking was not a prominent process during rifting of the SKR upper crust, in contrast with those applied to more mature magma-rich segments in the Main Ethiopian rift (Ebinger & Casey, 2001; Keranen et al., 2004; Rooney et al., 2005; Bastow et al., 2008). The immature nature of the SKR system is also argued from the temporal development of its border and inner fault networks. The assessment that the inner fault network partly (Natron) or nearly totally (Magadi) developed in response to a hangingwall flexuring process along the Sambu/Natron and E/Nguruman border fault system (Muirhead et al., 2016) necessarily implies that: i) border fault and inner fault activities partly overlapped in time during the late rifting stage, ii) border fault activity was not abandoned since initial faulting along the W/Nguruman fault, 7 Ma ago, iii) no sharp transition from border fault- to intra-rift fault-dominated strain accommodation existed during the 7 Ma-lasted history of the SKR system, and iv) the SKR system has not yet reached the 'Main Ethiopian Rift' mature stage that resulted in the inward focussing of deformation and its achievement through exclusively inner faulting and associated magmatic dyking (Ebinger, 2005; Keir et al., 2006; Corti, 2009; Agostini et al., 2011). However, magmatic processes are assumed to have accompanied recent rifting processes in the SKR system at depth, beneath the rift axis, where melt zones and ascending magmas might have triggered intra-rift faulting (Muirhead et al., 2016; Lee et al., 2017).

5.2. Structural inheritance and synrift strain/magmatism

It has long been established that the NW/SE transverse fault pattern in the highly segmented North-Central Kenya rift nucleated along reactivated Proterozoic shear zones during Tertiary extension (Chorowicz, 1989; Smith and Mosley, 1993; Ring, 1994; Le Turdu et al., 1999; Le Gall et al., 2000; Hautot et al., 2000; Le Gall et al., 2005; Vétel and Le Gall, 2006). Similarly-trending transverse faults are very few in the SKR under study, i.e. the Kordjya fault in Fig. 2B (Muirhead & Kattenhorn, 2018), which is instead cross-cut by transverse structures consistently oriented NE/SW (Sonjo, Engare/Eyasi and Crater Highlands). Their origin, structural significance and causal mechanisms are discussed below in a coherent tectonic model about rift propagation at the Tanzanian craton margin.

5.2.1. Inherited origin of the Engare-Eyasi lineament

It has been assessed above that the Engare-Eyasi lineament resulted from the multistage and segmented reactivation of a >200 km-long inherited discontinuity during Neogene-Recent times. Basement surface geology supplies no clear evidence about the initial nature of this inferred discontinuity. The folded and generally shallowly-dipping attitude of the foliation plane in the Proterozoic basement host-rocks (i.e. the granulite belts of Fritz et al., 2009) indicates that

Proterozoic ductile strain exerted no control on the orientation of the Engare-Eyasi lineament. The latter more likely roots at a greater depth along a steeply-dipping discontinuity, presumably Archaean in age, that might correlate with similarly-oriented structures identified as suture-related features on gravimetry modelling in the Eyasi-Mbulu area, further SW (Fig. 10A) (Fletcher et al., 2018). According to this interpretation, the eastern edge of the Tanzanian craton should extend beneath the westerly-translated Proterozoic thrust-nappe pattern as far east as the Engare-Eyasi lineament. This is in agreement with the structural sections of Fritz et al. (2009) which show Proterozoic thrust terranes rooting eastwards into a steep crustal ramp, ca 200 km east of the exposed frontal thrust (Fig. 10A). The various types of rift structures aligned along the Engare-Eyasi discontinuity imply that its rejuvenation under the regional EW extension might have not operated by simple extensional reactivation and was instead achieved by a combination of processes, possibly controlled by the thermal state of the crust. This is supported by the specific distribution of: i) brittle strain at its two extremities (Engare and Eyasi faults), i.e. on the rift flanks where the crust was colder, whereas ii) tectono-magmatic structures took place as either minor diking along the Gelai-Naibor Soito axis or prominent intrusions in the Central Highlands, i.e. in the hotter and axial rifted crust (Fig. 10C). The importance of the Engare-Eyasi discontinuity is further argued by its NE prolongation, away from the rift axis, into the >200 km-long morphological structure bounding the Narok-Nairobi-Mount Kenya volcanic plateaus and which likely formed as a pre-rift topography, in response to plume-induced uplift of the East African plateau in Miocene times (> 13 Ma) (Wichura et al., 2010).

5.2.2. Causal mechanisms of the OOB offset rift block

The structural development of the OOB offset block, on the western flank of the SKR axial trough, can be satisfactorily explained in two different, but not mutually-exclusive ways. The first hypothesis is based on the temporal and spatial correlations displayed by the Sonjo and Engare transverse structures that both initiated early, probably in the time-range 7-1.3 Ma, and at the same latitude (Figs. 2, 3). Thus, it can be envisaged that, in response to the narrowing (up to 20 km) of the Natron basin caused by the Engare salient, the rifted domain shifted westwards *via* the Sonjo transfer zone into the 40 km-wide OOB offset block, in order to maintain a nearly constant border fault aspect ratio along-strike (fault throw *vs* hangingwall width dimension). According to the second scenario, the W/Nguruman border fault propagated as far south as 2°45’ 45’ where its intersection with the Engare-Eyasi transverse discontinuity resulted in a triangle-shaped hangingwall block, the kinematics of which primarily depends on two parameters that are: i) the opposite *vs* similar dip directions of the two intersecting faults and ii) their acute *vs* obtuse angle (Fig. 12A) (Lezzar et al., 2002; Vétel & Le Gall, 2006). In the present case, the acute angle of the two structures and their

respective dip attitude (easterly-facing for the W/Nguruman and (inferred) steeply-dipping for the Engare/Eyasi) are unfavourable conditions for any downthrow of the proto-Natron hangingwall block (Fig. 12B1). In these conditions, the arrest of the southerly-propagating W/Nguruman fault induced the shift of strain backwards to the NW along the Sonjo/OOF fault network (Fig. 12B2).

5.2.3. Off-axis magmatism and strain initiation in the Crater Highlands

With respect to the general southerly-propagating SKR-NTD rift framework, the Crater Highlands magmatic range is unusual in that: i) it occurs in an off-axis position, ii) its NE/SW trend is oblique to the submeridian rift axis, and iii) its magmatism is younging northeastwards from the Lemagrut (5 Ma), Sadiman (4 Ma) and Ngorongoro (3.7 Ma) volcanoes to the Olmoti (1.6 Ma), Loolmalasin (1.2 Ma) and Embagai (0.5 Ma) edifices (Figs. 13A, B) (Bagdasaryan et al., 1973; McIntyre et al., 1974; Manega, 1993; Foster et al., 1997). Initiation of off-axis magmatism in an outermost position, close to the exposed eastern edge of the Tanzanian craton, and its later migration towards the Natron rift axis to the NE (Le Gall et al., 2008; Mana et al., 2015), are here attributed to three interacting processes that are: (Figs. 13C, D): i) the deflection of ascending plume-related mantle melts beneath the thick lithospheric root of the craton, in agreement with the 3D-thermo-mechanical numerical models of Koptev et al. (2016, 2018) and the scenario applied to the Rungwe volcanic province further south in relation to the Bangwelu craton (Grijalva et al., 2018), ii) their uprising along one topographic step at the base of the cratonic lithosphere, iii) the lateral channelling of mantle flow along NE/SW-oriented transverse zones of thinned lithosphere (Fletcher et al., 2018), and finally, iv) the migration of associated magmas through the upper crust along similarly-oriented weakness zones that guided the NE/SW alignment of eruptive centres at the surface in the Crater Highlands. At the base of the lithosphere, the rift pattern displays a number of NE/SW thinned zones branching eastwards along a NS one (Fletcher et al., 2018). It might continue beneath the Natron axial trough and connect with the ~50 km-wide and NE/SW infra-lithospheric antiform-like structure identified on receiver function modelling, parallel to the Engare-Eyasi linament (Fig. 10D) (Plasman et al., 2017). Lateral channelling of asthenosphere upwelling, at a high angle (about 40°) to the submeridian SKR rift axis, implies a major decoupling between the two structural levels, with increased control of the regional tectonic stress in the upper crust. A quite similar heterogeneous crust/lithosphere pattern is documented about off-axis magmatic ranges in the Main Ethiopian rift (Bastow et al., 2008; Corti, 2012; Rooney et al., 2014; Chiasera et al., 2018).

Magmatic segments are known to constitute potential strain nucleation sites in response to lithospheric thermal weakening (Callot et al., 2002; Bialas et al., 2010). The location of the Eyasi fault, immediately SW of the Sadiman-Lemagrut-Ngorongoro zone of initial volcanism in the Crater Highlands, suggests that its nucleation <3.1 Ma ago (Foster et al., 1997) was triggered by thermal

softening of the lithosphere during early magmatism (5-3 Ma) at the SW edge of the nascent volcanic range (Fig. 13C). A similar process likely occurred later (<1.2 Ma) at its NE end (Foster et al., 1997) and promoted the southerly propagation of the Natron bounding fault through the initially stiff Engare-Eyasi discontinuity (as suggested above), and then its linkage with the Manyara fault.

6. Conclusions

New insights into mechanisms of rifting at the South Kenya/North Tanzania boundary are provided by integrating the following into a coherent structural model: i) the relatively well-known Magadi-Natron axial trough, ii) the much less investigated Ol Doinyo Ogol offset block (both forming the SKR), and iii) the western part of the NTD, i.e. the Crater Highlands, Eyasi and Manyara rift arms. The main contributions of our work consist as follow:

- A two-stage rift model is applied to the 7 Ma-lasted SKR system based on: i) relative timing constraints supplied by the contrasted topography of its bounding fault network on SRTM-30 satellite imagery, and ii) available age dataset of synrift volcanics.

- The early rift stage (7-1.3 Ma) is dominated by initiation of the highly-segmented proto-Magadi-OOB-Natron half-graben basins along the W/Nguruman-OOF dextrally offset bounding fault system.

- The southerly propagation of early rifting resulted in the diachronous emplacement of flood-type lavas from the Magadi (7 Ma-old Lengitoto trachytes) to the OOB (3.5 Ma-old Salei basalts) fault-bounded basins. However, earlier initiation of rifting at a pre-volcanic stage (> 7 Ma) is inferred from available geophysically-imaged basement depths in the Magadi basin.

- Pronounced changes in the style of rifting occurred during the younger rift stage (1.3 Ma-Present) and resulted in the inward focussing of strain *via:* i) the easterly shift of border fault activity from the OOF to the Sambu-Natron fault and from the W/ to E/Nguruman fault, and ii) intra-rift faulting that accommodated, for the first time, part of the regional extension in the linear and narrower Magadi-Natron axial trough.

- The quantitative analysis of extension shows that: i) upper crustal extension achieved by brittle strain in the 7 Ma-lasted SKR rift system is maximal (7.2-6.2 km, 11.6-9.2 %) in the Magadi segment, where most of extension (89-82 %) was primarily accommodated though displacements along the rift bounding fault network during a long-lived process that nearly spanned the lifetime of the evolving rift basins, but with a marked decrease of activity through time. ii) From the modest amount of intra-rift fault-related extension during the recent rift stage (<1.3 Ma, 22-15 % and 18-11 % in the Natron and Magadi segments, respectively), it is argued that inner faulting was not the dominant mode of

strain accommodation in the SKR rift during inward focussing of strain, and that no sharp transition exists from border fault- to intra-rift fault-dominated strain accommodation over time, as typically observed in immature rift segments. iii) The significant contribution of the OOB offset block (2.4-0.8 %) to the total extension recorded by the Natron/OOB composite southern segment (6.0-3.9 %) demonstrates its necessary integration into any kinematic model to avoid biasing quantitative estimate of bulk strain in part of the SKR.

- The influence of crustal inheritance in the SKR-NTD rift system is emphasized about the inferred Engare-Eyasi transverse discontinuity to which is attributed: i) the arrest, lateral jump and transfer of strain in the Ol Doinyo Ogol offset block, and ii) the oblique (NE-SW) trajectory of the colinear Eyasi branch and off-axis Crater Highlands volcanic range.

Acknowledgments

This work is part of a PhD thesis program (RG) that was partially funded by the French Embassy in Dar Es Salaam. The help and assistance of the ambassadors and administrative staff (both previous and current), L. Crayssac, P. Boncour, E. Drillet, P. Camy, F. Reynes and V. Lengyel, is greatly appreciated. Field investigations (may 2017) in the Natron-OOB area were funded by 'Geosciences Océan' UMR/CNRS 6538 Brest, IUEM Brest, Pr. P. Tarits (GO Brest) and C. Tiberi (CNRS Montpellier, France). Many thanks to the driver Kelvin (Fortes) and the Masai guide Olomeloki Tall for their assistance in the field. We are grateful to Dr. Alessandro Tibaldi, one anonymous referee and the Editor for providing thorough comments that helped improving the clarity of the manuscript. Richard Mejida (UBO Brest), Mrs Danielle Skuy and Pr. Ron (Djibouti) are thanked for improving the english.

References

Agostini, A., Bonini, M., Corti, G., Sani, F., Mazzarini, F., 2011. Fault architecture in the Main Ethiopian Rift and comparison with experimental models: Implications for rift evolution and Nubia-Somalia kinematics. Earth Planet. Sci. Lett., 301, 479-492.

Aki, K., 1979. Characterization of barriers on an earthquake fault. J. Geophys. Res., 84, B11, 6140-6148.

Albaric, J., Deverchère, J., Petit, C., Perrot, J., Le Gall, B., 2009. Crustal rheology and depth distribution of earthquakes: insights from the central and southern East African Rift System. Tectonophysics, 468, 1-4, 28-41.

Albaric, J., Perrot, J., Deverchère, J., Deschamps, A., Le Gall, B., Wambura, R., Petit, C., Tiberi, C., Sue, C., Songo, M., 2010. Contrasted seismogenic and rheological behaviours from shallow and

deep earthquake sequences in the North Tanzanian Divergence, East Africa. J. Afr. Earth Sci., 58, 5, 799-811.

Albaric, J., Deverchère, J., Perrot, J., Jakovlev, A., Deschamps, A., 2014. Deep crustal earthquakes in North Tanzania, East Africa: Interplay between tectonic and magmatic processes in an incipient rift. Geochem. Geophys. Geosyst., 15, 374-394.

Baer, G., Hamiel, Y., Shamir, G., Nof, R., 2008. Evolution of a magma-driven earthquake swarm and triggering of the nearby Ol Doinyo Lengai eruption, as resolved by InSAR, ground observations and elastic modelling, East African Rift. Earth Planet. Sci. Lett., 272, 1-2, 339-352.

Bagdasaryan, G., Gerasimovskiy, V., Polykov, A., Gukasyan, R., 1973. Age of volcanic rocks in the rift zones of East Africa. Geokhimiya, 1, 84-90.

Baker, B., 1958. Geology of the Magadi area. Geol. Surv. Kenya Report, 42, 81 pp.

Baker, B., Williams, L., Miller, J., Fitch, F., 1971. Sequence and geochronology of the Kenya rift volcanics. Tectonophysics, 11, 191-215.

Baker, B., Mitchell, J., Williams, L., 1988. Stratigraphy, geochronology and volcanotectonic evolution of the Kedong-Naivasha-Kinangop region, Gregory Rift Valley, Kenya. J. Geol. Soc., London, 145, 107-116.

Balestrieri, M., Bonini, M., Corti, G., Sani, F., Philippon, M., 2016. A refinement of the chronology of rift-related faulting in the Broadly Rifted Zone, southern Ethiopia, through apatite fission-track analysis. Tectonophysics, 671, 42–55.

Bastow, I., Nyblade, A., Stuart, G., Rooney, T., Benoit, M., 2008. Upper mantle seismic structure beneath the Ethiopian hot spot: Rifting at the edge of the African low-velocity anomaly: Geochem. Geophys. Geosystems, 9, 12, doi.org/10.1029/2008GC002107.

Bialas, R., Buck, W., Qin, R., 2010. How much magma is required to rift a continent? Earth Planet. Sci. Lett. 292, 68-78.

Birt, C., Maguire, P., Khan, M., Thybo, H., Keller, G., Patel, J., 1997. The influence of pre-existing structures on the evolution of the southern Kenya Rift Valley. Evidence from seismic and gravity studies. Tectonophysics, 278, 211-242.

Boone, S.C., Kohn, B., Andrew, A., C.K., Morley, Seiler, C., Foster, D., 2019. Birth of the East African Rift System: Nucleation of magmatism and strain in the Turkana Depression. Geology, 47, 9, 886-890.

Burgmann, R., Pollard, D., Martel, S., 1994. Slip distributions on faults: effects of stress gradients, inelastic deformation, heterogeneous host-rock stiffness, and fault interaction. J. Struct. Geol., 16, 1675-1690.

Calais, E., d'Oreye, N., Albaric, J., Deschamps, A., Delvaux, D., Deverchère, J., Ebinger, C., et al., 2008. Strain accommodation by slow slip and diking in a youthful continental rift, East Africa. Nature, 456, 783-787.

Callot, J.P., Geoffroy, L., Brun, J.P., 2002. Development of volcanic margins: three dimensional laboratory models. Tectonics, 21, doi:10.1029/2001TC901019.

Chapman, G., Lippard, S., Martyn, J., 1978. The stratigraphy and structure of the Kamasia Range, Kenya Rift Valley. J. Geol. Soc., London, 135, 265-281.

Chiasera, B., Rooney, T., Girard, G., Yirgu, G., Grosfils, E., Ayalew, D., Mohr, P., Zimbelman, J., Ramsey, M., 2018. Magmatically-assisted off-rift extension - the case for broadly distributed strain accommodation. Geosphere, 14, 4, 1544-1563.

Chorowicz, J., 1989. Transfer and transform fault zones in continental rifts: examples in the Afro-Arabian rift system. Implications of crust breaking. J. Af. Earth Sci., 8, 203-214.

Corti, G., 2008. Control of rift obliquity on the evolution and segmentation of the main Ethiopian rift. Nature Geosci., 1, 258-262.

Corti, G., 2009. Continental rift evolution: From rift initiation to incipient break-up in the Main Ethiopian Rift, East Africa. Earth-Sci. Rev. 96, 1-53.

Corti, G., 2012, Evolution and characteristics of continental rifting: Analog modelling-inspired view and comparison with examples from the East African Rift System. Tectonophysics, 522-523, 1-33.

Crossley, R., 1979. The Cenozoic stratigraphy and structure of the western part of the Rift Valley in southern Kenya. J. Geol. Soc., London, 136, 4, 393-405.

Dawers, N., Anders, M., Scholz, C., 1993. Growth of normal faults: displacement-length scaling. Geology, 21, 1107-1110.

Dawers, N., Anders, M., 1995. Displacement-length scaling and fault linkage. J. Struct. Geol., 17, 607-614.

Dawson, J., 1992. Neogene tectonics and volcanicity in the North Tanzania sector of the Gregory Rift Valley: contrasts with the Kenya sector. Tectonophysics, 204, 1/2, 81-83.

Delvaux, D, Barth, A., 2010. African stress from formal inversion of focal mechanism data. Tectonophysics, 482, 105-128.

Dundass, D., Awadalla, G., 1966. Loliondo geological map, 1:125 000, Quarter degree sheet 16 & 27, Geol. Surv. Tanzania, Dodoma.

Ebinger, C., 2005. Continental breakup: the East African perspective. Astronomy & Geophysics, 46, 2.16-2.21.

Ebinger, C., Deino, A., Drake, R., Tesha, A., 1989. Chronology of volcanism and rift propagation: Rungwe volcanic province, East Africa. J. Geoph. Res., 94, 15,785-15,803.

Ebinger, C., Casey, M., 2001. Continental breakup in magmatic provinces: an Ethiopian example. Geology, 29, 527-530.

Ebinger, C., Poudjom Djomani, Y., Mbede, E., Foster, A., Dawson, J., 1997. Rifting Archaean lithosphere: Eyasi-Manyara-Natron rifts, East Africa. J. Geol. Soc., London, 154, 947-960.

Ebinger, C., Yemane, T., Harding, D., Tesfaye, S., Kelley, S., Rex, D., 2000. Rift deflection, migration, and propagation: linkage of the Ethiopian and Eastern rifts, Africa. GSA Bull. 112 (2), 163-176.

Fairhead, J., Mitchell, J., Williams, L., 1972. New K/Ar determinations on rift volcanics of S. Kenya and their bearing on age of rift faulting. Nature Physic. Sci., 238, 66-69.

Fletcher, A., Abdelsalam, M., Emishaw, L., 2018. Lithospheric controls on the rifting of the Tanzanian craton at the Eyasi basin, Eastern branch of the East African rift system. Tectonics, 37, 9, 2818-2832.

Foster, A., Ebinger, C., Mbede, E., Rex, D., 1997. Tectonic development of the northern Tanzanian sector of the East African Rift System. J. Geol. Soc., London, 154, 689-700.

Fritz, H., Tenczer, V., Hauzenberger, C., Wallbrecher, E., Muhongo, S., 2009. Hot granulite nappes - Tectonic styles and thermal evolution of the Proterozoic granulite belts in East Africa. Tectonophysics, 477, 3-4, 160-173.

Grijalva, A., Nyblade, A., Homman, K., Accardo, N., Gaherty, J.B., Ebinger, C., et al., 2018. Seismic evidence for plume- and craton-influenced upper mantle structure beneath the Northern Malawi rift and the Rungwe volcanic province, East Africa. Geochem. Geophys. Geosyst., 19, 10, 3980-3994.

Hautot, S., Tarits, P., Wheeler, K., Le Gall, B., Tiercelin, J.J., Le Turdu, C., 2000. Deep structure of the Baringo Rift Basin (central Kenya) from three-dimensional magnetotelluric imaging: implications for rift evolution. J. Geophys. Res., 105, 23,493-23,518.

Ibs-von Seht, M., Blumenstein, S., Wagner, R., Hollnack, D., Wohlenberg, J., 2001. Seismicity, seismotectonics and crustal structure of the southern Kenya Rift - new data from the Lake Magadi area. Geophys. J. Intern., 146, 2, 439-453.

Isaac, G. 1965. The stratigraphy of the Peninj Beds and the provenance of the Natron Australopithecine mandibule. Quaternaria, 7, 101-130.

Isaac, G., Curtis, G., 1974. Age of early Acheulian industries from the Peninj Group, Tanzania. Nature, 249, 624-627.

Isola, I., Mazzarini, F., Bonini, M., Corti, G., 2014. Spatial variability of volcanic features in early-stage rift settings: the case of the Tanzania Divergence, East African rift system. Terra Nova, 26, 6, 461-468.

Keir, D., Bastow, I., Corti, G., Mazzarini, F., Rooney, T., 2015. The origin of along-rift variations in faulting and magmatism in the Ethiopian Rift. Tectonics, 34, 3, 464-477.

Keir, D., Ebinger, C., Stuart, G., Daly, E., Ayele, A., 2006. Strain accommodation by magmatism and faulting as rifting proceeds to breakup: Seismicity of the Northern Ethiopian Rift. J. Geophys. Res., 111, B05314, doi:10.1029/2005JB003748.

Keranen, K., Klemperer, S., Gloaguen, R., and the EAGLE Working Group. 2004. Three-dimensional seismic imaging of a protoridge axis in the Main Ethiopian Rift. Geology, 32, 949-952.

Kervyn, M., Ernst, G., Harris, A., Belton, F., Mbede, E., Jacobs, P., 2008. Thermal remote sensing of the low-intensity carbonatite volcanism of Oldoinyo Lengai, Tanzania. Intern. J. Remote Sensing, 29, 6467–6499, doi:10 .1080 /01431160802167105.

Kim, Y., Sanderson, D., 2005. The relationship between displacement and length of faults: a review. Earth-Sci. Rev., 68, 317-34.

King, B., 1978. Structural evolution of the Gregory rift valley. In: Bishop, W. (Ed.), Geological Background to Fossil Man, 6, Geol. Soc., London, 29-45.

Koptev, A., Burov, E., Calais, E., Leroy, S., Gerya, T., Guillou, L. Cloetingh, S., 2016. Contrasted continental rifting via plume-craton interaction: Applications to Central East African rift. Geoscience Frontiers, 7, 2, 221-236.

Koptev, A., Cloetingh, S., Gerya, T., Calais, E., Leroy, S., 2018. Non-uniform splitting of a single mantle plume by double cratonic keels: Insights into the origin of central and southern East African Rift System. Terra Nova, 30, 2, 125-134.

Lee, H., Fischer, T., Muirhead, J., Ebinger, C., Kattenhorn, S., Sharp, Z., Kianji, G., Sano, Y., Takahata, N., 2017. Incipient rifting accompanied by the release of subcontinental lithospheric mantle volatiles in the Magadi and Natron basin, East Africa. J. Volcanol. Geotherm. Res., doi:10.1016/j.jvolgeores.2017.03.017.

Le Gall, B., Tiercelin, J.J., Richert, J.P., Gente, P., Sturchio, N., Stead, D., Le Turdu, C., 2000. A morphotectonic study of an extensional fault zone in a magma-rich rift: The Baringo Trachyte fault system, central Kenya Rift. Tectonophysics, 320, 87-106.

Le Gall, B., Gernigon, L., Rolet, J., Ebinger, C., Gloaguen, R., Nilsen, O., Dypvik, H., Deffontaines, B., Mruma, A., 2004. Neogene-Holocene rift propagation in central Tanzania: morphostructural and aeromagnetic evidence from the Kilombero area. Bull. Geol. Soc. Am., 116, 490-510.

Le Gall, B., Vétel, W., Morley, C., 2005. Inversion tectonics during continental rifting: The Turkana Cenozoic rifted zone, northern Kenya. Tectonics, 24, TC2002, doi:10.1029/2004TC001637.

Le Gall, B., Nonnotte, P., Rolet, J., Benoit, M., Guillou, H., Mousseau-Nonnotte, M., Albaric, J., Deverchère, J., 2008. Rift propagation at craton margin: distribution of faulting and volcanism in the North Tanzanian Divergence (East Africa) during Neogene times. Tectonophysics, 448, 1-19.

Le Turdu, C., Richert, J.P., Xavier, J.P., Renaut, R., Tiercelin, J.J., Rolet, J., Lezzar, K., Coussement, C., 1999. Influence of preexisting oblique discontinuities on the geometry and evolution of extensional fault patterns: Evidence from the Kenya Rift using SPOT imagery. In Morley, C., (ed.), Geoscience of Rift Systems. Evolution of East Africa. AAPG. Studies in Geology, 44, 173-191.

Lezzar, K., Tiercelin, J.J., Cohen, A., Reynolds, D., Le Gall, B., Scholz, C., 2002. Control of normal fault interaction on the distribution of major Neogene sedimentary depocenters, Lake Tanganyika, East African rift. AAPG. Bull., 86, 1027-1059.

Macheyeki, A., Delvaux, D., De Batist, M., Mruma, A., 2008. Fault kinematics and tectonic stress in the seismically active Manyara-Dodoma Rift segment in Central Tanzania - Implications for the East African Rift. J. Af. Earth Sc., 51, 4, 163-188.

Mana, S., Furman, T., Turrin, B., Feigenson, M., Swisher, C., 2015. Magmatic activity across the East African North Tanzanian Divergence Zone. J. Geol. Soc., London, 172, 368-389.

Manega, P. 1993. Geochronology, geochemistry and isotopic study of the Plio-Pleistocene hominid sites and the Ngorongoro Volcanic Highland in northern Tanzania. PhD. thesis, Univ. Colorado.

McHenry, L., Luque, L., Gomez, J., Diez-Martın, F., 2011. Promise and pitfalls for characterizing and correlating the zeolitically altered tephra of the Pleistocene Peninj Group, Tanzania. Quat. Res., 75, 3, 708-720.

McIntyre, R., Mitchell, J., Dawson, J., 1974. Age of fault movements in the Tanzanian sector of the East African Rift system. Nature, 247, 354-356.

Ministry of Energy and Regional development of Kenya, 1987. Geological map of Kenya, 1:1, 000 000. (Eds) BEICIP, Rueil-Malmaison, France.

Möller, A., Mezger, K., Schenk, V., 2000. U-Pb dating of metamorphic minerals: Pan-African metamorphism and prolonged slow cooling of high pressure granulites in Tanzania, East Africa. Precambrian Res., 104, 123-146.

Morley, C., 1988. Variable extension in Lake Tanganyika. Tectonics, 7, 4, 785-801.

Morley, C., 1999. Aspects of transfer zone geometry and evolution in East Africa rifts. AAPG. Bull., 83, 161-171.

Morley, C., Wescott, W., Stone, D., Harper, R., Wigget, S., Karanja, F., 1992. Tectonic evolution of northern Kenya Rift. J. Geol. Soc., 149, 333-348.

Mosley, P., 1993, Geological evolution of the late Proterozoic Mozambique Belt of Kenya. Tectonophysics, 221, 223-250.

Mugisha, F., Ebinger, C., Strecker, M., Pope, D., 1997. Two-stage rifting in the Kenya Rift: Implications for half-graben models. Tectonophysics, 278, 61-81.

Muirhead, J., Kattenhorn, S., Lee, H., Fischer, T., Mana, S., Turrin, B., Kianji, G., Dindi, E., Stamps, D., 2016. Evolution of upper crustal faulting assisted by magmatic volatile release during early-stage continental rift development in the East African Rift. Geosphere, 12, 1670, doi:10.1130/GES01375.1.

Muirhead, J., Kattenhorn, S., 2018. Activation of preexisting transverse structures in an evolving magmatic rift in East Africa. J. Struct. Geol., 106, 1-18.

Mulibo, G., Nyblade, A., 2016. The seismotectonics in Southeastern Tanzania: Implications for propagation of the eastern branch of the East African Rift. Tectonophysics, 676, 20-30.

Nicol, A., Walsh, J., Watterson, J., Gillespie, P., 1996. Fault size distributions–are they really power-law? J. Struct. Geol., 18, 2-3, 191-197.

Nonnotte, P., Guillou, H., Le Gall, B., Benoit, M., Cotten, J., Scaillet, S., 2008. New K-Ar age determinations of Kilimanjaro volcano in the North Tanzanian diverging rift, East Africa. J. Volcan. Geoth. Res., 173, 1-2, 99-112.

O'Donnell, J., Adams, A., Nyblade, A., Mulibo, G., Tugume, F., 2013. The uppermost mantle shear wave velocity structure of eastern Africa from Rayleigh wave tomography: constraints on rift evolution. Geophys. J. Int., 194, 2, 961-978.

Peacock, D., 1991. Displacements and segment linkage in strike-slip fault zones. J. Struct. Geol., 13, 1025-1035.

Pik, R., Marty, B., Carignan, J., Yirgu, G., Ayalew, T., 2008. Timing of East African Rift development in southern Ethiopia: Implication for mantle plume activity and evolution of topography. Geology, 36(2), 167-170.

Plasman, M., Tiberi, C., Ebinger, C., Gautier, S., Albaric, J., Peyrat, S., Deverchère J., Le Gall, B. et al., 2017. Lithospheric low-velocity zones associated with a magmatic segment of the Tanzanian Rift, East Africa. Geophys. J. Int., 210, 1, 465-481.

Plasman, M., Hautot, S., Tarits, P., Gautier, S., Tiberi, C., Le Gall, B., Mtelela, K., Gama, R., 2019. Lithospheric structure of a transitional magmatic to amagmatic continental rift system : Insights from a 3-D Magnetotelluric study in the North Tanzanian Divergence, Geosciences, 9, Doi: 10.3390/geosciences9110462.

Pollard, D., Segall, P., 1987. Theoretical displacements and stresses near fractures in rock: with applications to faults, joints, veins, dikes, and solution surfaces. In: Atkinson, B. (ed.), Fracture Mechanics of Rock. Acad. Press, London, 277-349.

Ring, U., 1994. The influence of preexisting structure on the evolution of the Cenozoic Malawi rift (East African rift system). Tectonics, 13, 313-326.

Ritsema, J., Nyblade, A.A., Owens, T., Langston, C., VanDecar, J., 1998. Upper mantle seismic velocity structure beneath Tanzania, east Africa: Implications for the stability of cratonic lithosphère. J. Geophys. Res. Solid Earth, 103(B9), 21201–21213.

Roecker, S. Ebinger, C., Tiberi, C., Mulibo, R., Ferdinand, R., Mtelela, K., et al. 2017. Subsurface images of the Eastern rift, Africa, from the joint inversion of body waves, surface waves, and gravity: investigating the role of fluids in early-stage continental rifting. Geophys. J. Int., 210, 931–950.

Rooney, T., Furman, T., Yirgu, G., Ayalew, D. 2005. Structure of the Ethiopian lithosphère : Xenolith evidence in the Main Ethiopian rift. Geochim. Cosmochim. Acta 69 (15), 3889-391.

Rooney, T., Bastow, I., Keir; D., Mazzarini, F., Movsesian, E. et al., 2014. The protracted development of focused magmatic intrusion during continental rifting. Tectonics, 33, 6, 875-897.

Rosendahl, B., 1987. Architecture of continental rifts with special reference to east Africa. Ann. Rev. Earth Plan. Sci., 15, 445-503.

Saria, E., Calais, E., Stamps, D., Delvaux, D., Hartnady, C., 2014. Present-day kinematics of the East African Rift. J. Geophys. Res., 119, 3584-3600.

Shackleton, R., 1993. Tectonics of the lower crust: a view from the Usambara Mountains, NE Tanzania. J. Struct. Geol., 15, 663-671.

Sherrod, D., Magigita, M., Kwelwa, S., 2013. Geologic map of Oldonyo Lengai and surroundings, Arusha region, United Republic of Tanzania. U.S. Geol. Surv. Open-File Report 2013-1306, 1:50,000, 50 p.

Sippel, J., Meessen, C., Cacace, M., Mechie, J., Fishwick, S., Heine, C., Scheck, M., Strecker, M., 2017. The Kenya rift revisited: insights into lithospheric strength through data-driven 3D gravity and thermal modelling. J. Geophys. Res., Solid Earth, 8, 1, 45-81.

Smith, M., Mosley, P., 1993. Crustal heterogeneity and basement influence on the development of the Kenya Rift, East Africa. Tectonics, 12, 591-606.

Thomas, R., Spencer, C., Bushi, A., Baglow, N., Boniface, N., de Kock, G., et al., 2016. Geochronology of the central Tanzania craton and its southern and eastern orogenic margins. Precambrian Res., 277, 47-67.

Thybo, H., Maguire, P., Birt, C., Perchuc, E., 2000. Seismic reflectivity and magmatic underplating beneath the Kenya Rift. Geophys. Res. Lett., 27, 2745-2748.

Tiberi, C., Gautier, S., Ebinger, C., Roecker, S., Plasman, M., Albaric, J., Peyrat, S., Déverchère, J., Perrot, J., et al., 2019. Lithospheric modification by extension and magmatism at the craton-orogenic boundary: North Tanzania Divergence, East Africa. Geophys. J. Int., 216, 1693-1710, doi:10.1093/gji/ggy521.

Van der Beek, P., Mbede, E., Andriessen, P., Delvaux, D., 1998. Denudation history of the Malawi and Rukwa rift flanks (East African rift system) from apatite fission track thermochronlogy. J. Af. Earth Sci., 26, 3, 363-385.

Vétel, W., Le Gall, B., Walsh, J., 2005, Geometry and growth of an inner rift fault pattern: The Kino Sogo Fault Belt, Turkana Rift (North Kenya). J. Struct. Geol., 27, 2204-2222.

Vétel, W., Le Gall, B., 2006. Dynamics of prolonged continental extension in magmatic rifts: the Turkana Rift case study (North Kenya). In: Yirgu, G., Ebinger, C., Maguire, P. (eds.), The Structure and Evolution of the East African Rift System in the Afar Volcanic Province. Geol. Soc. London, Sp. Pub., 259, 211-235.

Wheeler, W., Rosendahl, B., 1994. Geometry of the Livingstone mountains border fault, Nyasa (Malawi) rift, East Africa. Tectonics 13, 303-312.

Wichura, A., Bousquet, R., Oberhänsli, R., Strecker, M., Trauth, M., 2010. Evidence for Middle Miocene uplift of the East African Plateau. Geology, 38, 6, 543-546.

Weinstein, A., Oliva, S., Ebinger, C., Roecker, S., Tiberi, C., Aman, M., Lambert, C., Witkin, E., Albaric, J., Gautier, S., Peyrat, S., 2017. Fault-magma interactions during early continental rifting: seismicity of the Magadi-Natron-Manyara basins, Africa. Geochem. Geophys. Geosyst., doi.org/10.1002/2017GC007027.

Supporting information

Supplementary data available online.

Figure captions

Figure 1. Main structural and magmatic features in the South Kenya rift (SKR) and the North Tanzanian Divergence zone (NTD). A. Topo30 digital elevation model showing the distribution of topographic domes with relation to rift structures in East Africa. NTD., North Tanzanian Location of

Fig. 1A shown. B. Sketch map of major rift structures in the SKR-NTD system on a Topo30 DEM. CH., Crater Highlands; ET., Engaruka trough; MP., Mbulu plateau; OOB., Ol Doinyo Ogol block; TKV., Tarosero-Kilimanjaro volcanic chain. The dashed line is the trace of the boundary between the Tanzanian craton and the Proterozoic belts. C. Sketch map showing regional-scale structural disturbances (in red) with respect to the archetypal and linear arrangement of the SKR (in green). Same abbreviations as in Fig. 1B. ES., Engare salient; EF., MF., NF., OOF., PF., SNF., Eyasi, Manyara, Nguruman, Ol Doinyo Ogol, Pangani, Sambu-Natron fault, respectively. CH., TKV., Crater Highlands and Tarosero-Kilimanjaro magmatic chains.

Figure 2. Geology of the South Kenya rift. A. SRTM-30 DEM showing the offset rift pattern with the Ol Doinyo Ogol block on the western flank of the Natron axial trough. LM., Lake Magadi; KF., NF., NgF., OOF., SF., SnF., Kordjya, Natron, Nguruman, Ol Doinyo Ogol, Sambu, Sanjan fault, respectively; Volcanoes: E., Embagai; G., Gelai; K., Ketumbeine; Ke., Kerimasi; L., Lenderut; Lo., Loolmalsin; M., Mosonik; O., Olorgesailie; OL., Ol Doinyo Lengai; Om., Olmati; OS., Ol Doinyo Sambu; S., Shompole. The trace of 12 cross-sections ($A_{1\text{-}12}$) and 2 oblique sections (5C1, 2) discussed in the text is drawn. The western course of sections $A_{8\text{-}12}$ through the OOB is drawn in red. The red points mark the trace of the magnetotelluric profile discussed in Section 4.1.1. B. Corresponding simplified geological map. Same abbreviations as in Fig. 2A. The trace of sections 2C, D_1, D_2 is shown. C. Rift-parallel topographic profile showing the along-strike morphological segmentation of the axial floor. Vertical exaggeration = 14. $D_{1\text{-}2}$. Geological cross-sections in the Magadi (D_1) and Natron (D_2) segments. Vertical exaggeration = 5. Same colours as in Fig. 2B. Location in Figs. 2B and 5A ($D_1 = A_2$, $D_2 = A_{10}$).

Figure 3. Field views of rift structures in the Ol Doinyo Ogol offset block. Location in Fig. 2B. A. Stratified lacustrine limestones (slightly tilted to the south) overlying Proterozoic metamorphic rocks in the immediate hangingwall of the OOF border fault, at the northern extremity of the OOB offset basin. B. Brecciated facies of possibly hydrothermal origin. C. Incised topography of the OOF border fault in the background. Photo taken from the limestone site. D. Scree and landslide deposits at the foot of the Natron border fault. The Salei basaltic flows are slightly tilted to the SW in the fault scarp.

Figure 4. Conventional rules used in this work for estimating fault length and fault scarp elevations. A. Length measurement of a segmented fault. The length of the fault is significantly longer than its tip-to-tip length. B. Geometrical attributes of an eroded topographic fault profile. No scale.

Figure 5. Map-distribution and cross-sectional geometry of the normal fault network in the South Kenya rift. A. Map trace of the extensional fault grid (and corresponding numbers) extracted from the SRTM-30 DEM. The position of 12 parallel and regularly-spaced (10 km) cross-sections ($A_{1\text{-}12}$), used for extension estimates, is shown. ENF., East/Nguruman fault; Ge., Gelai; KTF., Kordjya fault; L.,

Lenderut; LM., Lake Magadi; M. Mosonik; NF., Natron fault; NP., Narok plateau; OL., Olorgesaille; OOB., Ol Doinyo Ogol block; OS., Ol Doinyo Sambu; SF., Sambu fault; Sh., Shombole; WNF., West/Nguruman fault. B. Six (over the twelve) morphostructural cross-sections showing marked changes in structural style from the Magadi ($A_{1\text{-}2\text{-}4}$) to the Natron ($A_{7\text{-}10\text{-}12}$) segments. Vertical exaggeration = 5. C. Two transverse morphostructural sections across the Sonjo transfer fault zone, showing (apparent) extensional faults. Vertical exaggeration = 5. Location in Fig. 2A.

Figure 6. Geometrical attributes of the inner fault population in the Magadi-Natron trough. A1. Focused SRTM-30 DEM showing the morphological expression of a narrow and highly-segmented, asymmetric half-graben, south of the Olorgesaile volcano. Location in Fig. 5A. The trace of sections A2 and A3 is shown. A2-3. Two topographic cross-profiles showing its asymmetrical morphology with increasing flank uplift to the east. Vertical exaggeration = 10. Location in Fig. A1. B. Histogram of inner fault azimuth (n = 140 data). C. Log-log plot of maximal displacement (D_{max}) *vs* fault length (L). The length and maximum displacement values of the 140 analyzed faults are shown in Supplemental Materials (Table S1).

Figure 7. Rift-parallel sketch section showing the composite dataset (geophysically-derived basement depths, topographic elevations and syntectonic volcanics thickness) used to calculate cumulative throws on the 110 km-long Nguruman-Sambu-Natron border fault system. ($A_{1\text{-}12}$ transects are located in Fig. 5A). See text for explanations. Same colours as in Fig. 2B.

Figure 8. Diagrams showing the along-strike distribution of cumulative extension in the 110 km-long SKR system from 12 regularly-spaced (10 km) cross-sections $A_{1\text{-}12}$ shown in Fig. 5A. A. Extension estimates related to: i) early rift-bounding faults (blue curve), ii) younger rift-bounding faults (yellow curve), and iii) inner faults (black curve). Extension values on bounding fault curves are represented by a midpoint and error bars related to the lower/upper estimates of footwall eroded material. B. Cumulative extension estimates related to inner faults (black curve) and bounding faults (green curve) in the Magadi-Natron half-graben. C. Cumulative extension estimates in: i) the Magadi-Natron half-graben (inner and border faults, blue curve), and ii) the entire SKR system (Magadi-Natron/OOB, red curve). D. Total extension (in %) in the entire SKR system. Excepted the inner fault curve, all extension profiles consistently show the segmentation of the SKR system into the Magadi and Natron segments at the transition zone $A_{5\text{-}7}$.

Figure 9. Structural evidence for a first-order transverse discontinuity crossing the SKR-NDT rift system from the Engare salient to the Eyasi fault. Earthquake distribution modified from Weinstein et al. (2017). Epicenters are colour coded with depth (in km) as follows: deep red (<5), red (<10), orange (<20), yellow (<30). Same abbreviations as in Figs. 2B, 5A. Es., Essimingor volcano. Inset shows a

pronounced morphological structure bounding the Narok-Nairobi-Mont Kenya Miocene lavas in the NE continuation of the Engare-Eyasi lineament (extracted from the Geological Map of Kenya, 1: 1,000,000, Ministry of Energy of Kenya, 1987). E., M., Eyasi and Manyara lakes, respectively; EED., Engare-Eyasi discontinuity; NP., Nairobi volcanic plateau.

Figure 10. Two-stage kinematic rift model of the SKR-NTD system during the last 7 Myrs. A. Pre-rift basement framework in map and cross-section. The traces of Archaean suture zones (crustal ramps) and Proterozoic thrusts (lines with triangles) are from Fletcher et al. (2018) and Fritz et al. (2009). The yellow area enclosed in dotted lines represents the future rifted domain. The Masai craton is not drawn. E., M., and N. are the Eyasi, Manyara and Natron lakes, shown as geographical coordinates. The trace of the cross-section is drawn north of the Masai craton (not shown). The rift pattern is not drawn on the section. B. Early rift stage (7-1.3 Ma) dominated by: i) the right-lateral offset of the SKR system in the OOB, ii) the arrest of fault propagation against the Engare-Eyasi transverse discontinuity, and iii) the off-axis emplacement of incipient magmatism in the Lenderut (L) (nascent Crater Highlands) and Essimingor (E) areas to the south. C. Late rift stage (<1.3 Ma) resulting in: i) inward focusing of strain in the linear and narrower Magadi-Natron axial trough, *via* the easterly migration of border faults and intra-rift faulting (not drawn), and ii) the southerly split of rifting along the Eyasi arm, in the SW course of the reactivated Engare-Eyasi discontinuity, and along the Manyara arm, in the southern extent of the Natron trough. D. Crustal architecture of the SKR-NTD rift system with transverse zones of thinned lithosphere disconnected from the upper crustal rift, compiled from Plasman et al. (2017) and Fletcher et al. (2018). Same abbreviations as in Figs. 1B, 2B.

Figure 11. Relative contribution of the main rift structures to total extension in the SKR system (in %).

Figure 12. Mechanisms of dextrally-offset rifting in South Kenya. A. Main geometrical parameters of two intersecting normal faults (angle and dip direction), modified from Vétel & Le Gall (2006). B. Kinematic model applied to the SKR fault system and implying: B1) the frontal arrest of the (extrapolated) W/Nguruman fault against the Engare-Eyasi transverse discontinuity, and B2) the shift of strain northwestwards *via* the Sonjo transfer fault zone. ES., Engare salient; OOB., Ol Doinyo Ogol block; OOF., Ol Doinyo Ogol fault; STF., Sonjo transfer fault zone; WNF., West/Nguruman fault.

Figure 13. Strain/magmatism relationships in the western part of the NTD. A. Major tectono-magmatic structures in the Eyasi and Crater Highlands (CH) areas, extracted from the SRTM-30 DEM in Fig. 2A. Same abbreviations as in Fig. 2A. B. Diagram showing the northeasterly younging of lavas in the off-axis Crater Highlands magmatic segment. Same abbreviations as in Fig. 9. C. Sketch map showing the location of the Eyasi and Manyara strain nucleation sites at the two extremities of the Crater Highlands (CH) range. D. 2D-model showing the vertical pathway of plume-related

melt/magma at the base of the step-like cratonic lithosphere (composite section based on the basement structural section in Fig. 10A).

Table captions

Table 1. Extension estimates calculated in terms of width ratio and % on the 12 cross-sections in the Magadi-Natron half-graben (A) and in the Natron/OOB system (B). See text for explanations about the maximum/minimum extension values related to the border fault networks and the total extension.

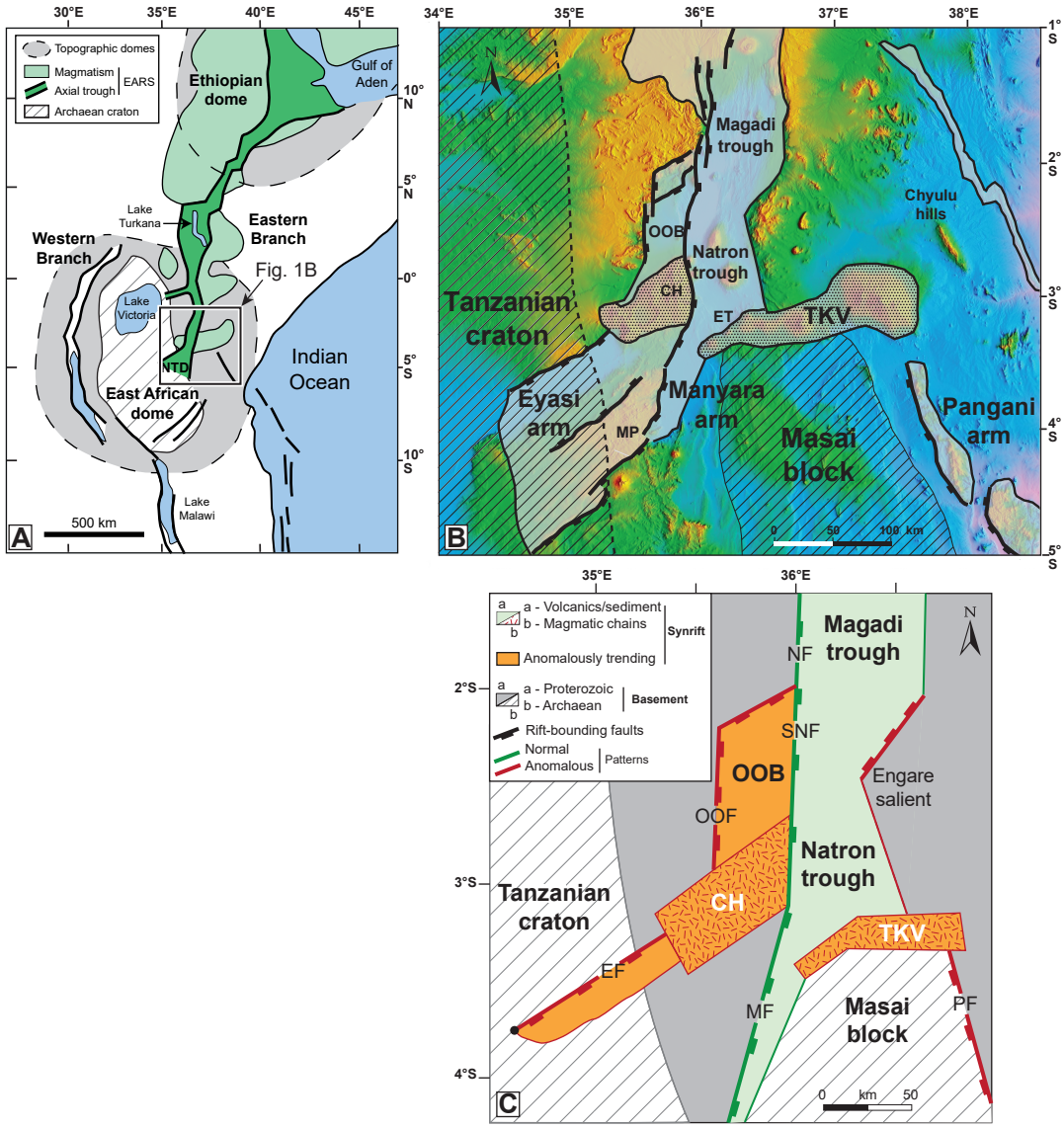

Figure 1. Main structural and magmatic features in the South Kenya rift (SKR) and the North Tanzanian Divergence zone (NTD). A. Topo30 digital elevation model showing the distribution of topographic domes with relation to rift structures in East Africa. NTD., North Tanzanian Location of Fig. 1A shown. B. Sketch map of major rift structures in the SKR-NTD system on a Topo30 DEM. CH., Crater Highlands; ET., Engaruka trough; MP., Mbulu plateau; OOB., Ol Doinyo Ogol block; TKV., Tarosero-Kilimanjaro volcanic chain. The dashed line is the trace of the boundary between the Tanzanian craton and the Proterozoic belts. C. Sketch map showing regional-scale structural disturbances (in red) with respect to the archetypal and linear arrangement of the SKR (in green). Same abbreviations as in Fig. 1B. ES., Engare salient; EF., MF., NF., OOF., PF., SNF., Eyasi, Manyara, Nguruman, Ol Doinyo Ogol, Pangani, Sambu-Natron fault, respectively. CH., TKV., Crater Highlands and Tarosero-Kilimanjaro magmatic chains.

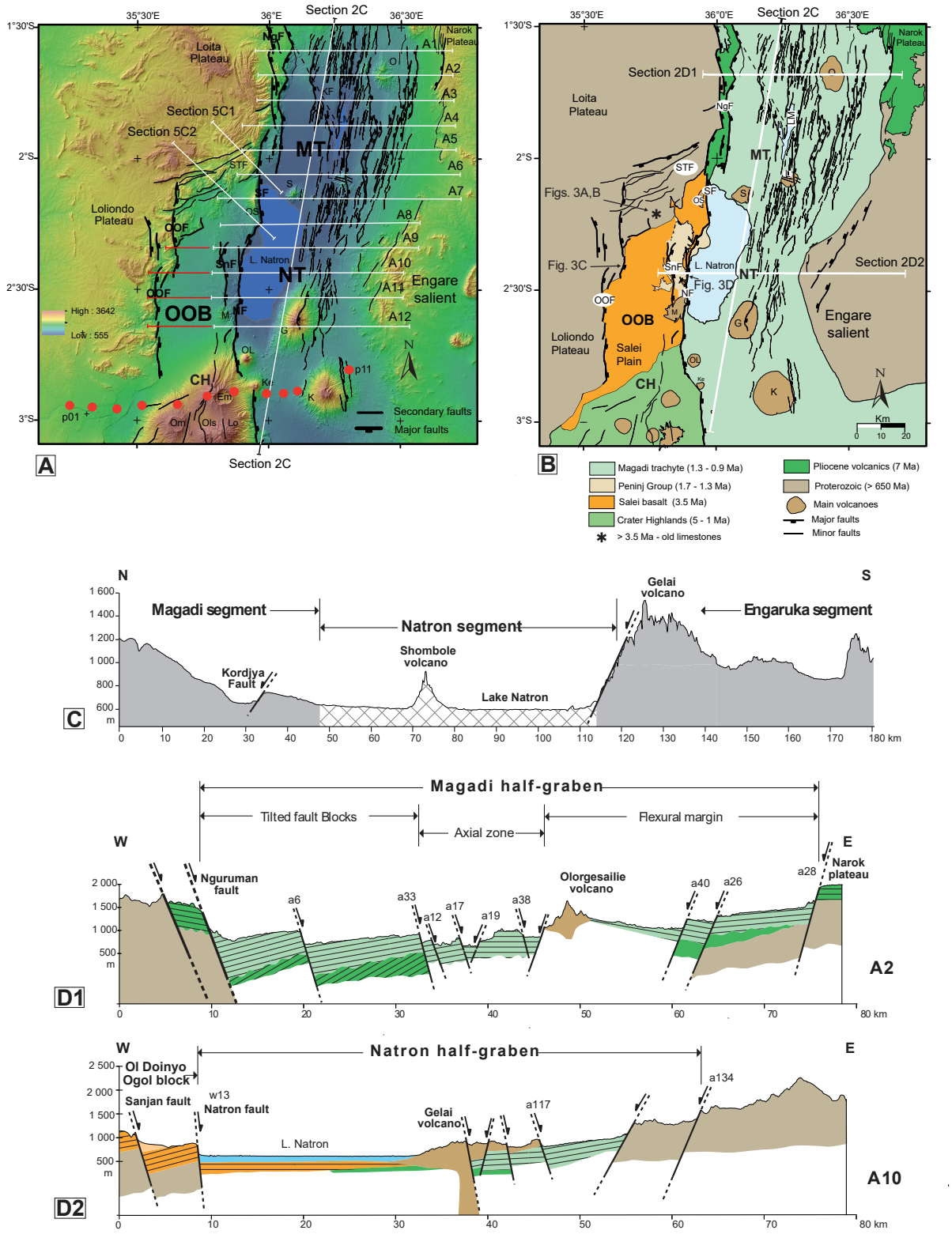

Figure 2. Geology of the South Kenya rift. A. SRTM-30 DEM showing the offset rift pattern with the Ol Doinyo Ogol block on the western flank of the Natron axial trough. LM., Lake Magadi; KF., NF., NgF., OOF., SF., SnF., Kordjya, Natron, Nguruman, Ol Doinyo Ogol, Sambu, Sanjan fault, respectively; Volcanoes: E., Embagai; G., Gelai; K., Ketumbeine; Ke., Kerimasi; L., Lenderut; Lo., Loolmalsin; M., Mosonik; O., Olorgesailie; OL., Ol Doinyo Lengai; Om., Olmati; OS., Ol Doinyo Sambu; S., Shompole. The trace of 12 cross-sections (A1-12) and 2 oblique sections (5C1, 2) discussed in the text is drawn. The western course of sections A8-12 through the OOB is drawn in red. The red points mark the trace of the magnetotelluric profile discussed in Section 4.1.1. B. Corresponding simplified geological map. Same abbreviations as in Fig. 2A. The trace of sections 2C, D1, D2 is shown. C. Rift-parallel topographic profile showing the along-strike morphological segmentation of the axial floor. Vertical exaggeration = 14. D1-2. Geological cross-sections in the Magadi (D1) and Natron (D2) segments. Vertical exaggeration = 5. Same colours as in Fig. 2B. Location in Figs. 2B and 5A (D1 = A2, D2 = A10).

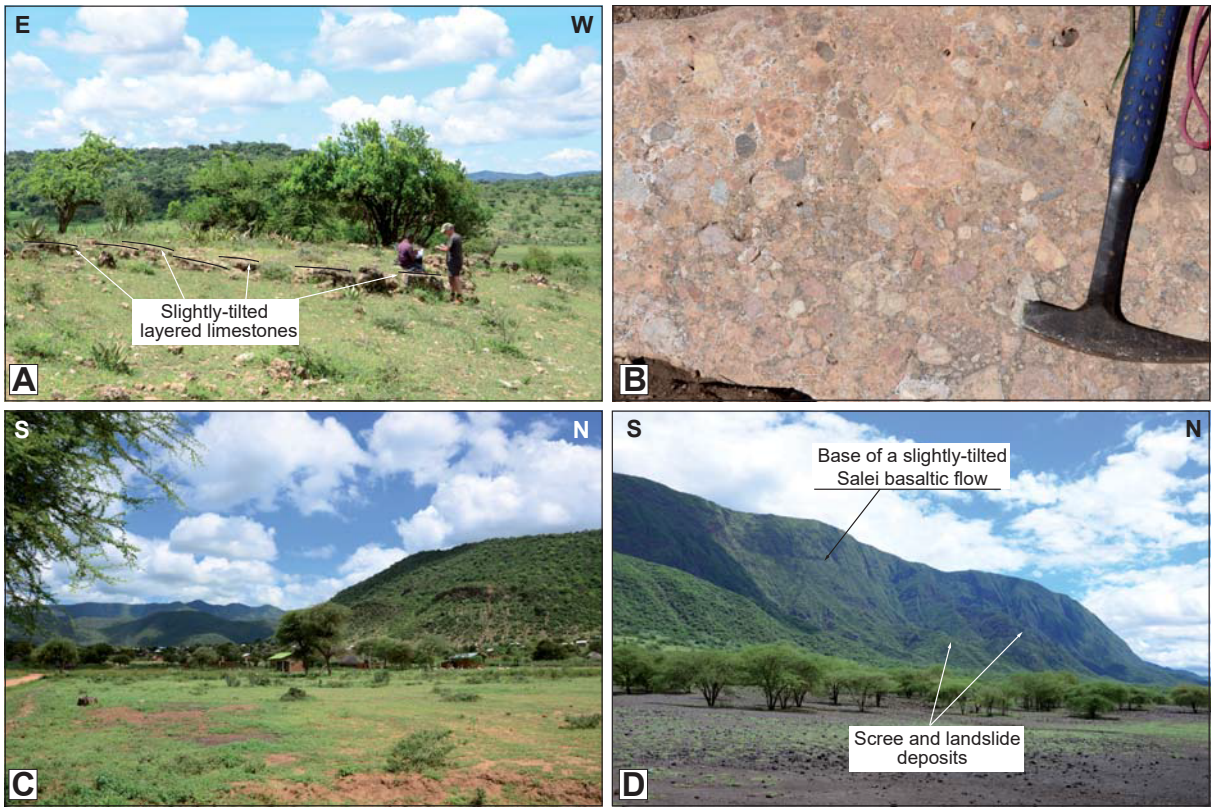

Figure 3. Field views of rift structures in the Ol Doinyo Ogol offset block. Location in Fig. 2B. A. Stratified lacustrine limestones (slightly tilted to the south) overlying Proterozoic metamorphic rocks in the immediate hangingwall of the OOF border fault, at the northern extremity of the OOB offset basin. B. Brecciated facies of possibly hydrothermal origin. C. Incised topography of the OOF border fault in the background. Photo taken from the limestone site. D. Scree and landslide deposits at the foot of the Natron border fault. The Salei basaltic flows are slightly tilted to the SW in the fault scarp.

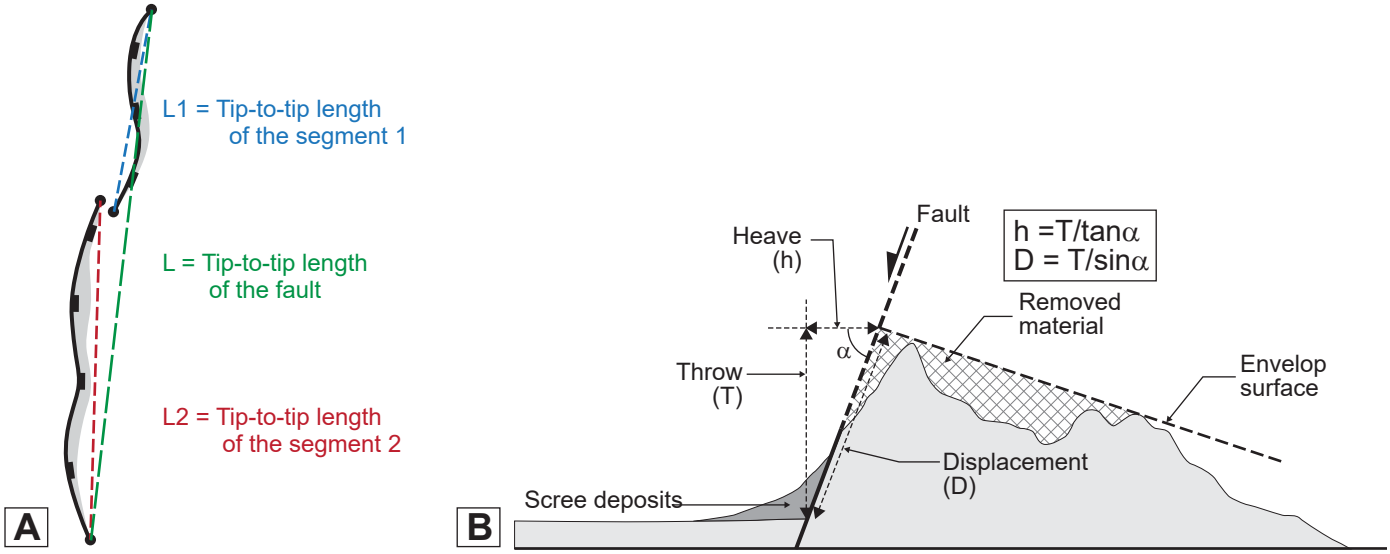

Figure 4. Conventional rules used in this work for estimating fault length and fault scarp elevations. A. Length measurement of a segmented fault. The length of the fault is significantly longer than its tip-to-tip length. B. Geometrical attributes of an eroded topographic fault profile. No scale.

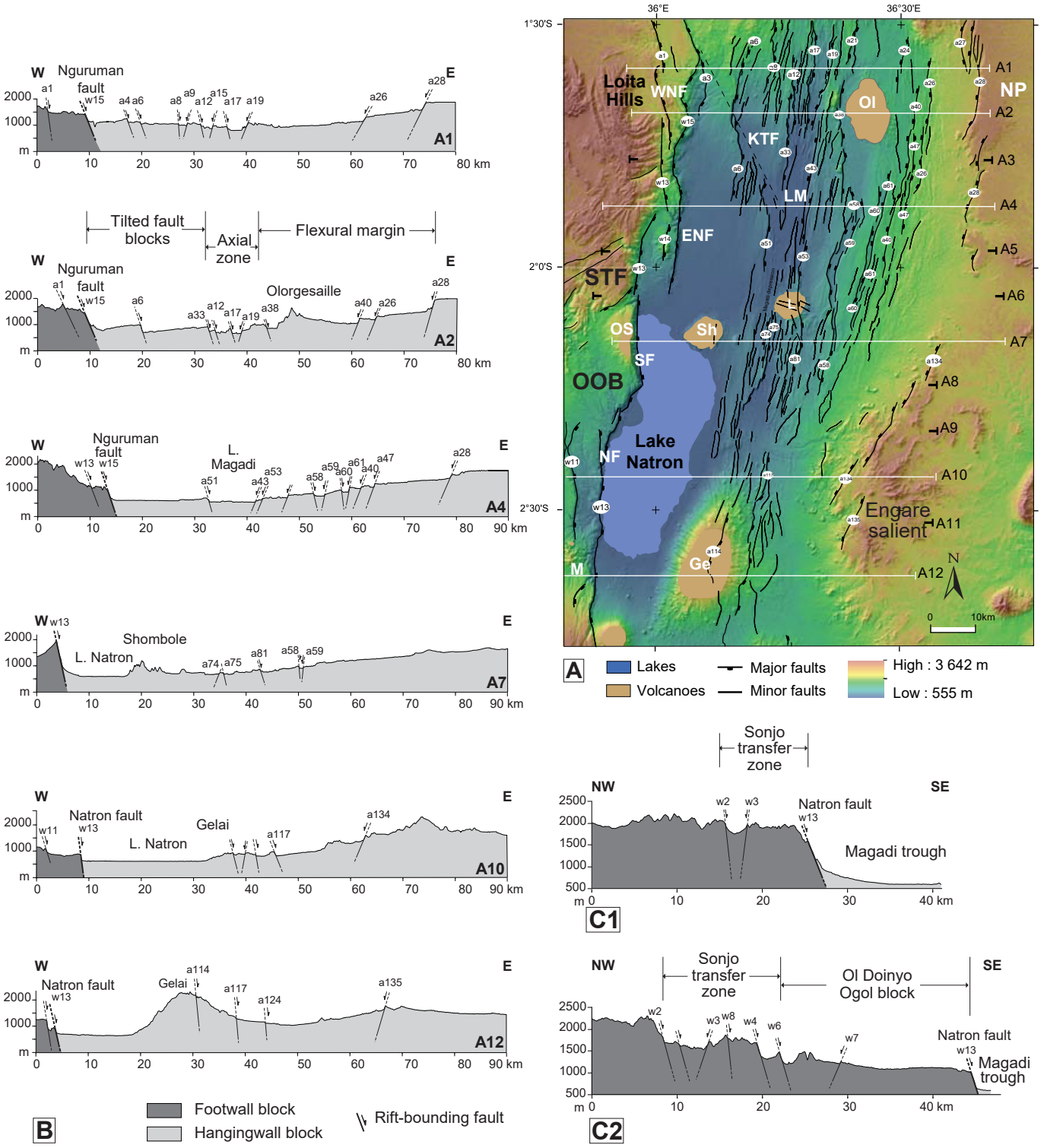

Figure 5. Map-distribution and cross-sectional geometry of the normal fault network in the South Kenya rift. A. Map trace of the extensional fault grid (and corresponding numbers) extracted from the SRTM-30 DEM. The position of 12 parallel and regularly-spaced (10 km) cross-sections (A1-12), used for extension estimates, is shown. ENF., East/Nguruman fault; Ge., Gelai; KTF., Kordjya fault; L., Lenderut; LM., Lake Magadi; M. Mosonik; NF., Natron fault; NP., Narok plateau; OL., Olorgesaille; OOB., Ol Doinyo Ogol block; OS., Ol Doinyo Sambu; SF., Sambu fault; Sh., Shombole; WNF., West/Nguruman fault. B. Six (over the twelve) morphostructural cross-sections showing marked changes in structural style from the Magadi (A1-2-4) to the Natron (A7-10-12) segments. Vertical exaggeration = 5. C. Two transverse morphostructural sections across the Sonjo transfer fault zone, showing (apparent) extensional faults. Vertical exaggeration = 5. Location in Fig. 2A.

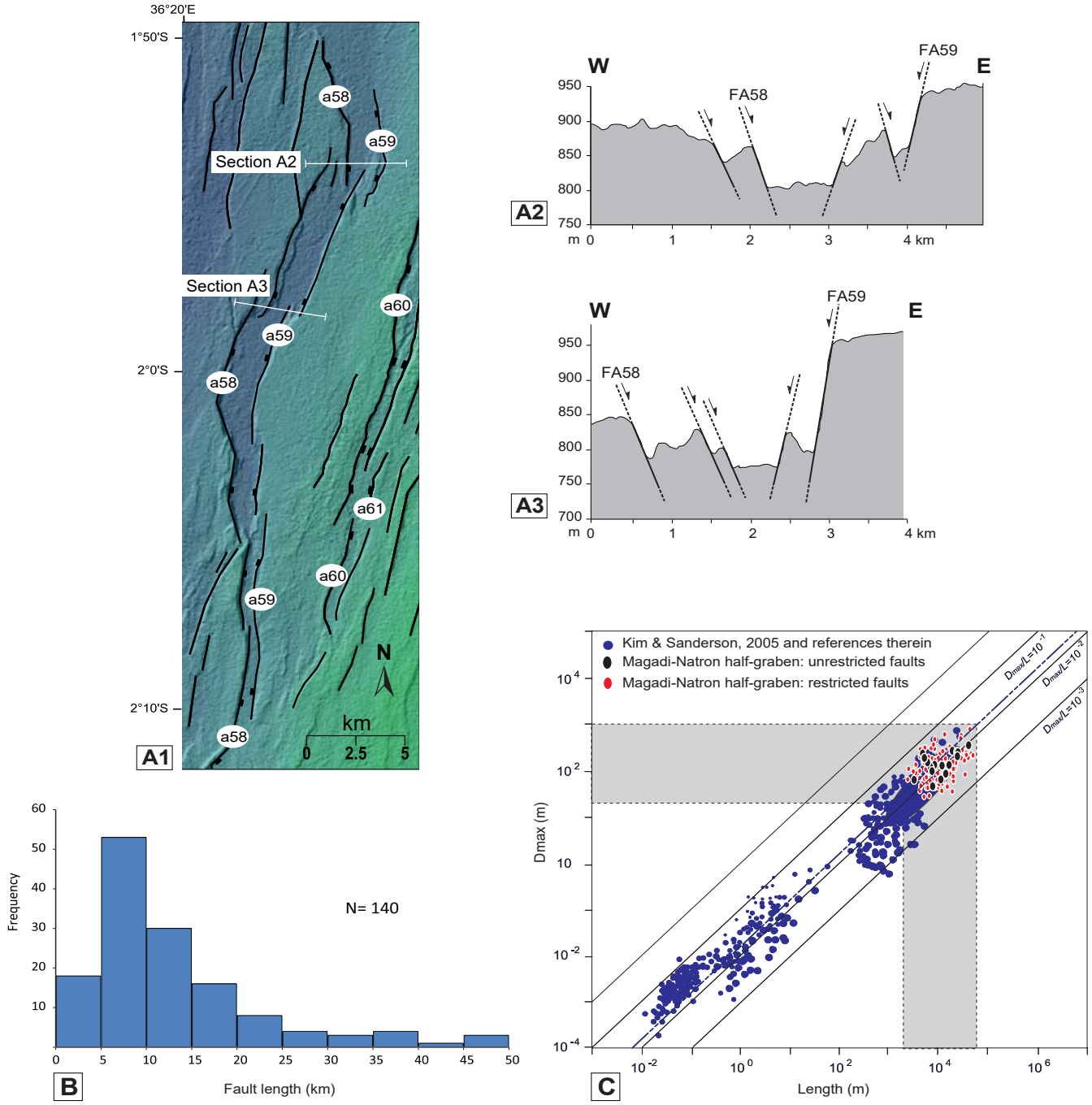

Figure 6. Geometrical attributes of the inner fault population in the Magadi-Natron trough. A1. Focused SRTM-30 DEM showing the morphological expression of a narrow and highly-segmented, asymmetric half-graben, south of the Olorgesaile volcano. Location in Fig. 5A. The trace of sections A2 and A3 is shown. A2-3. Two topographic cross-profiles showing its asymmetrical morphology with increasing flank uplift to the east. Vertical exaggeration = 10. Location in Fig. A1. B. Histogram of inner fault azimuth (n = 140 data). C. Log-log plot of maximal displacement (Dmax) vs fault length (L). The length and maximum displacement values of the 140 analyzed faults are shown in Supplemental Materials (Table S1).

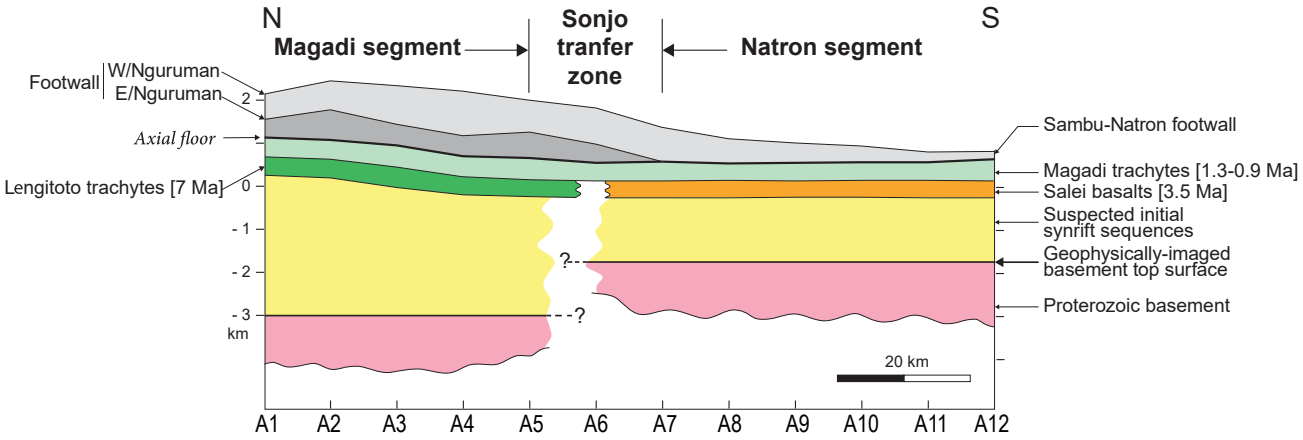

Figure 7. Rift-parallel sketch section showing the composite dataset (geophysically-derived basement depths, topographic elevations and syntectonic volcanics thickness) used to calculate cumulative throws on the 110 km-long Nguruman-Sambu-Natron border fault system. (A1-12 transects are located in Fig. 5A). See text for explanations. Same colours as in Fig. 2B.

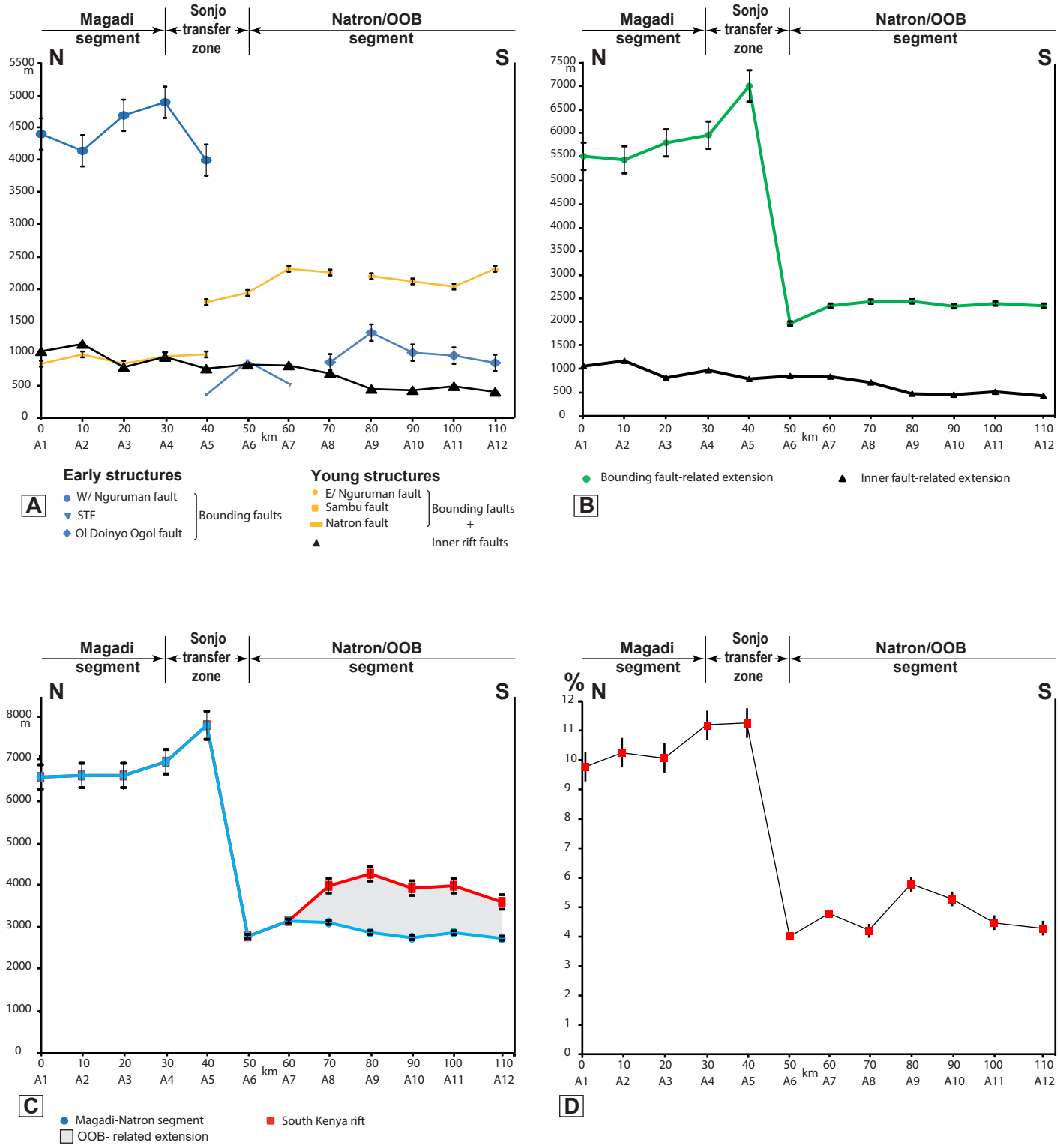

Figure 8. Diagrams showing the along-strike distribution of cumulative extension in the 110 km-long SKR system from 12 regularly-spaced (10 km) cross-sections A1-12 shown in Fig. 5A. A. Extension estimates related to: i) early rift-bounding faults (blue curve), ii) younger rift-bounding faults (yellow curve), and iii) inner faults (black curve). Extension values on bounding fault curves are represented by a midpoint and error bars related to the lower/upper estimates of footwall eroded material. B. Cumulative extension estimates related to inner faults (black curve) and bounding faults (green curve) in the Magadi-Natron half-graben. C. Cumulative extension estimates in: i) the Magadi-Natron half-graben (inner and border faults, blue curve), and ii) the entire SKR system (Magadi-Natron/OOB, red curve). D. Total extension (in %) in the entire SKR system. Excepted the inner fault curve, all extension profiles consistently show the segmentation of the SKR system into the Magadi and Natron segments at the transition zone A5-7.

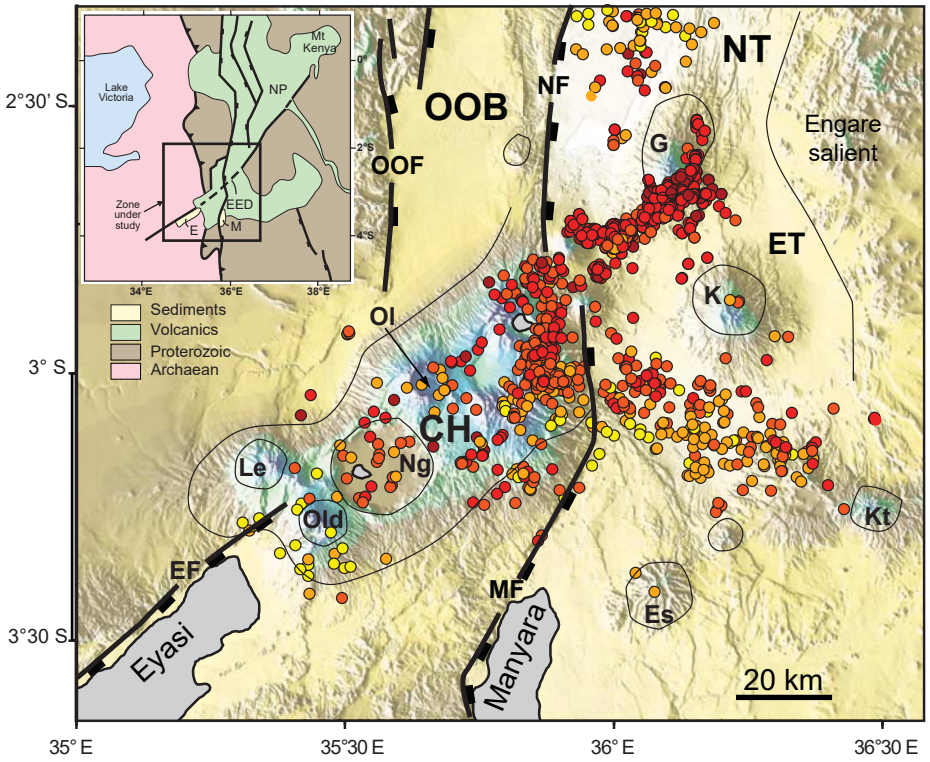

Figure 9. Structural evidence for a first-order transverse discontinuity crossing the SKR-NDT rift system from the Engare salient to the Eyasi fault. Earthquake distribution modified from Weinstein et al. (2017). Epicenters are colour coded with depth (in km) as follows: deep red (<5), red (<10), orange (<20), yellow (<30). Same abbreviations as in Figs. 2B, 5A. Es., Essimingor volcano. Inset shows a pronounced morphological structure bounding the Narok-Nairobi-Mont Kenya Miocene lavas in the NE continuation of the Engare-Eyasi lineament (extracted from the Geological Map of Kenya, 1: 1,000,000, Ministry of Energy of Kenya, 1987). E., M., Eyasi and Manyara lakes, respectively; EED., Engare-Eyasi discontinuity; NP., Nairobi volcanic plateau.

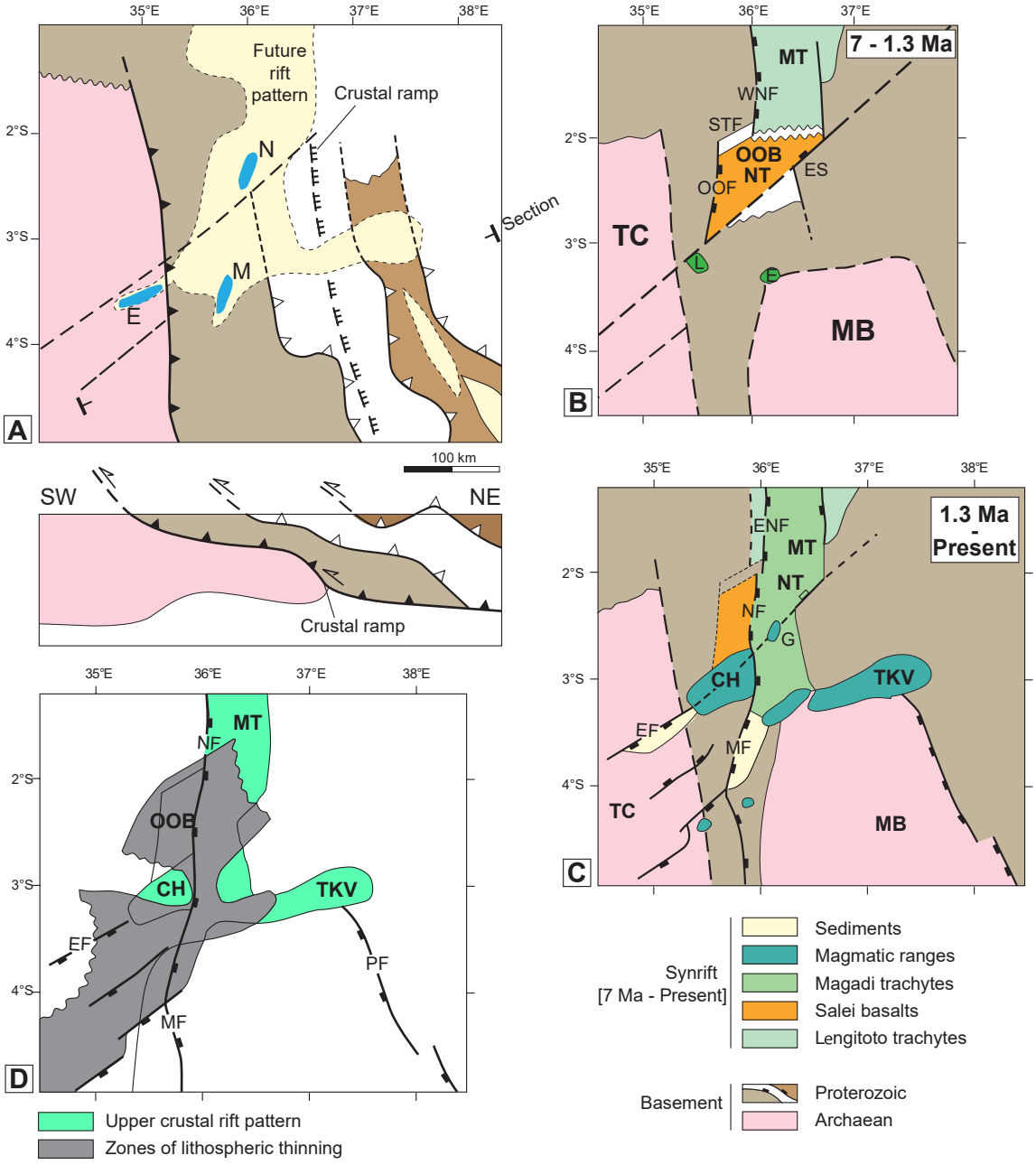

Figure 10. Two-stage kinematic rift model of the SKR-NTD system during the last 7 Myrs. A. Pre-rift basement framework in map and cross-section. The traces of Archaean suture zones (crustal ramps) and Proterozoic thrusts (lines with triangles) are from Fletcher et al. (2018) and Fritz et al. (2009). The yellow area enclosed in dotted lines represents the future rifted domain. The Masai craton is not drawn. E., M., and N. are the Eyasi, Manyara and Natron lakes, shown as geographical coordinates. The trace of the cross-section is drawn north of the Masai craton (not shown). The rift pattern is not drawn on the section. B. Early rift stage (7-1.3 Ma) dominated by: i) the right-lateral offset of the SKR system in the OOB, ii) the arrest of fault propagation against the Engare-Eyasi transverse discontinuity, and iii) the off-axis emplacement of incipient magmatism in the Lenderut (L) (nascent Crater Highlands) and Essimingor (E) areas to the south. C. Late rift stage (<1.3 Ma) resulting in: i) inward focusing of strain in the linear and narrower Magadi-Natron axial trough, via the easterly migration of border faults and intra-rift faulting (not drawn), and ii) the southerly split of rifting along the Eyasi arm, in the SW course of the reactivated Engare-Eyasi discontinuity, and along the Manyara arm, in the southern extent of the Natron trough. D. Crustal architecture of the SKR-NTD rift system with transverse zones of thinned lithosphere disconnected from the upper crustal rift, compiled from Plasman et al. (2017) and Fletcher et al. (2018). Same abbreviations as in Figs. 1B, 2B.

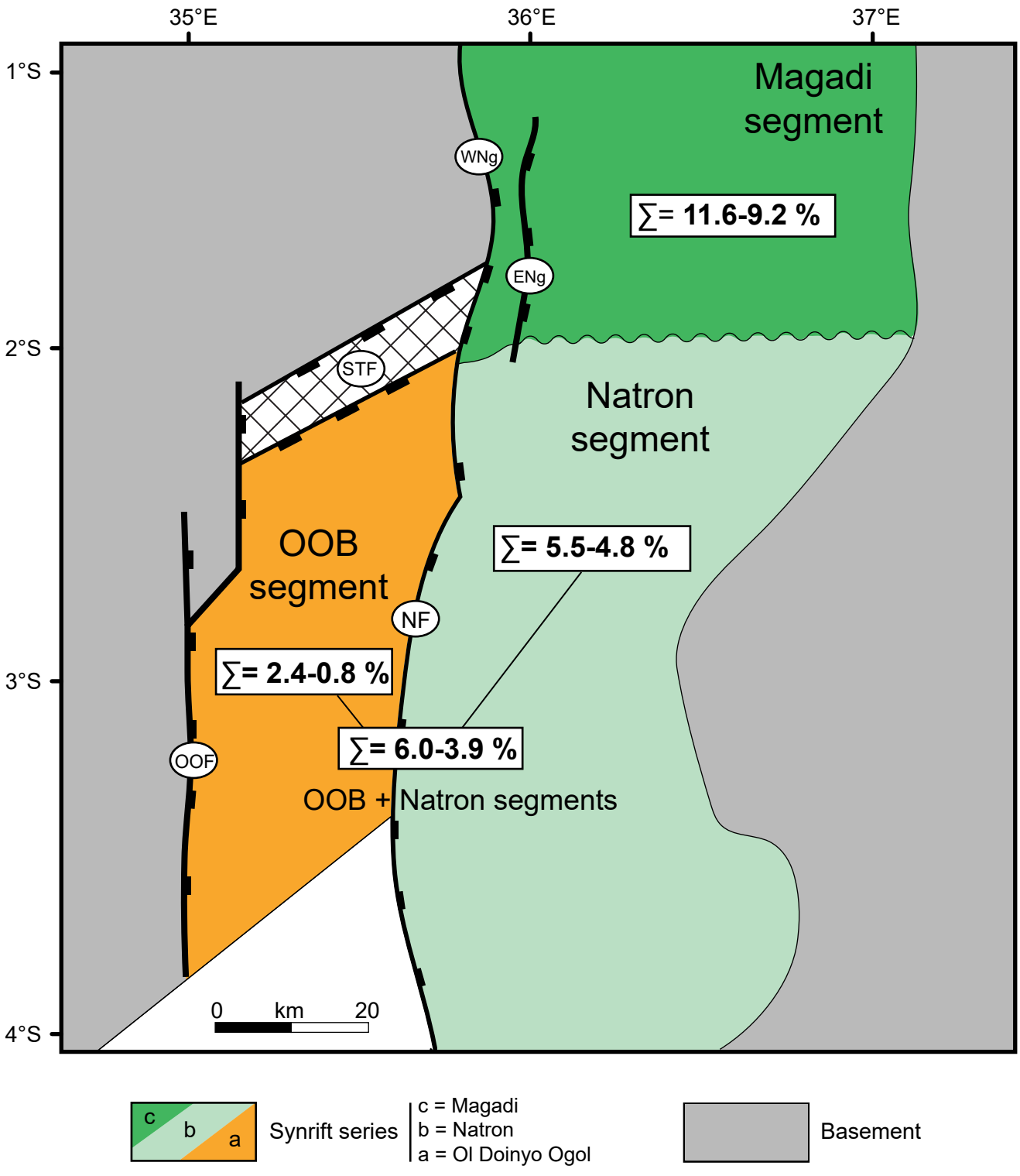

Figure 11. Relative contribution of the main rift structures to total extension in the SKR system (in %).

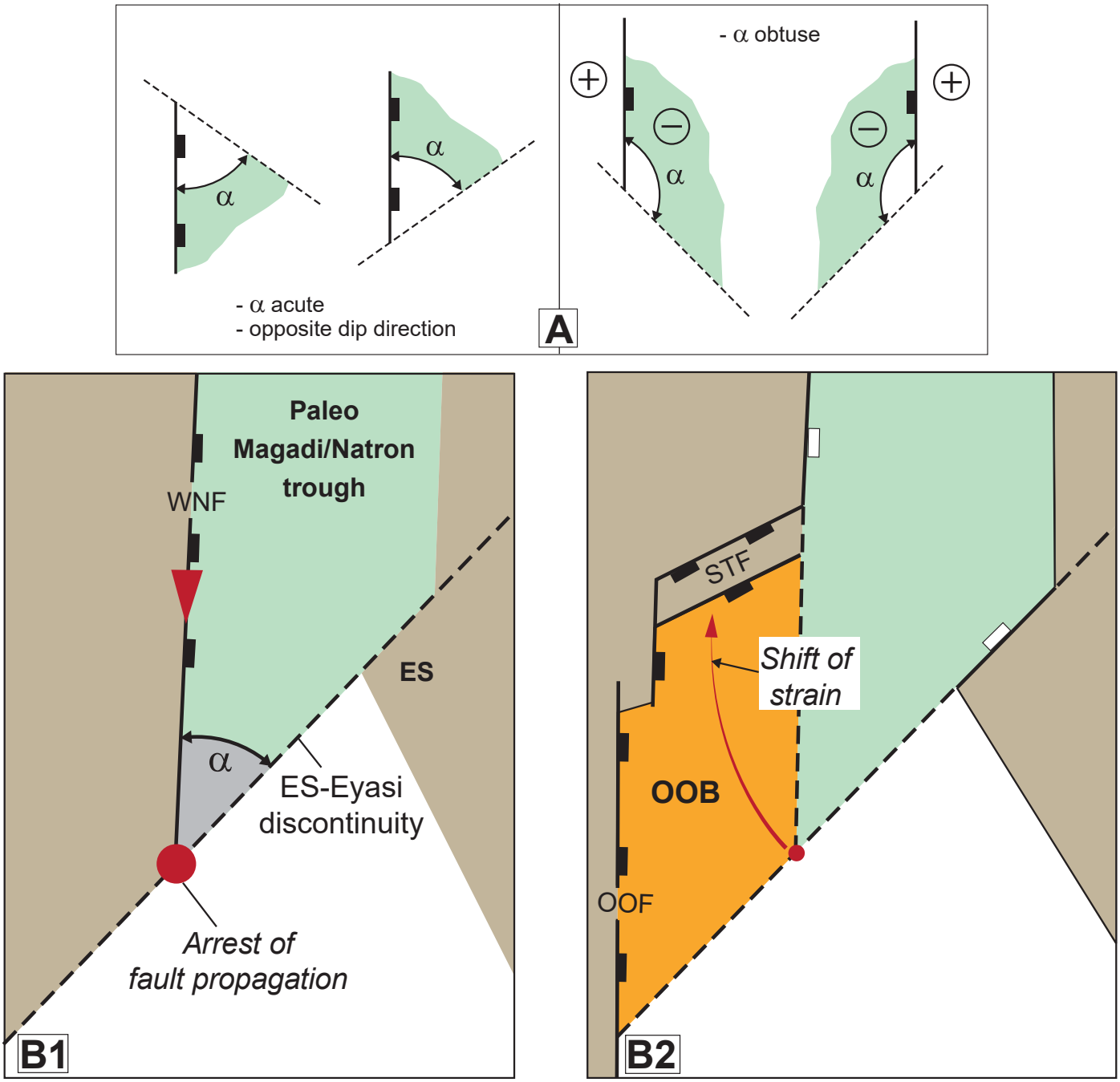

Figure 12. Mechanisms of dextrally-offset rifting in South Kenya. A. Main geometrical parameters of two intersecting normal faults (angle and dip direction), modified from Vétel & Le Gall (2006). B. Kinematic model applied to the SKR fault system and implying: B1) the frontal arrest of the (extrapolated) W/Nguruman fault against the Engare-Eyasi transverse discontinuity, and B2) the shift of strain northwestwards via the Sonjo transfer fault zone. ES., Engare salient; OOB., Ol Doinyo Ogol block; OOF., Ol Doinyo Ogol fault; STF., Sonjo transfer fault zone; WNF., West/Nguruman fault.

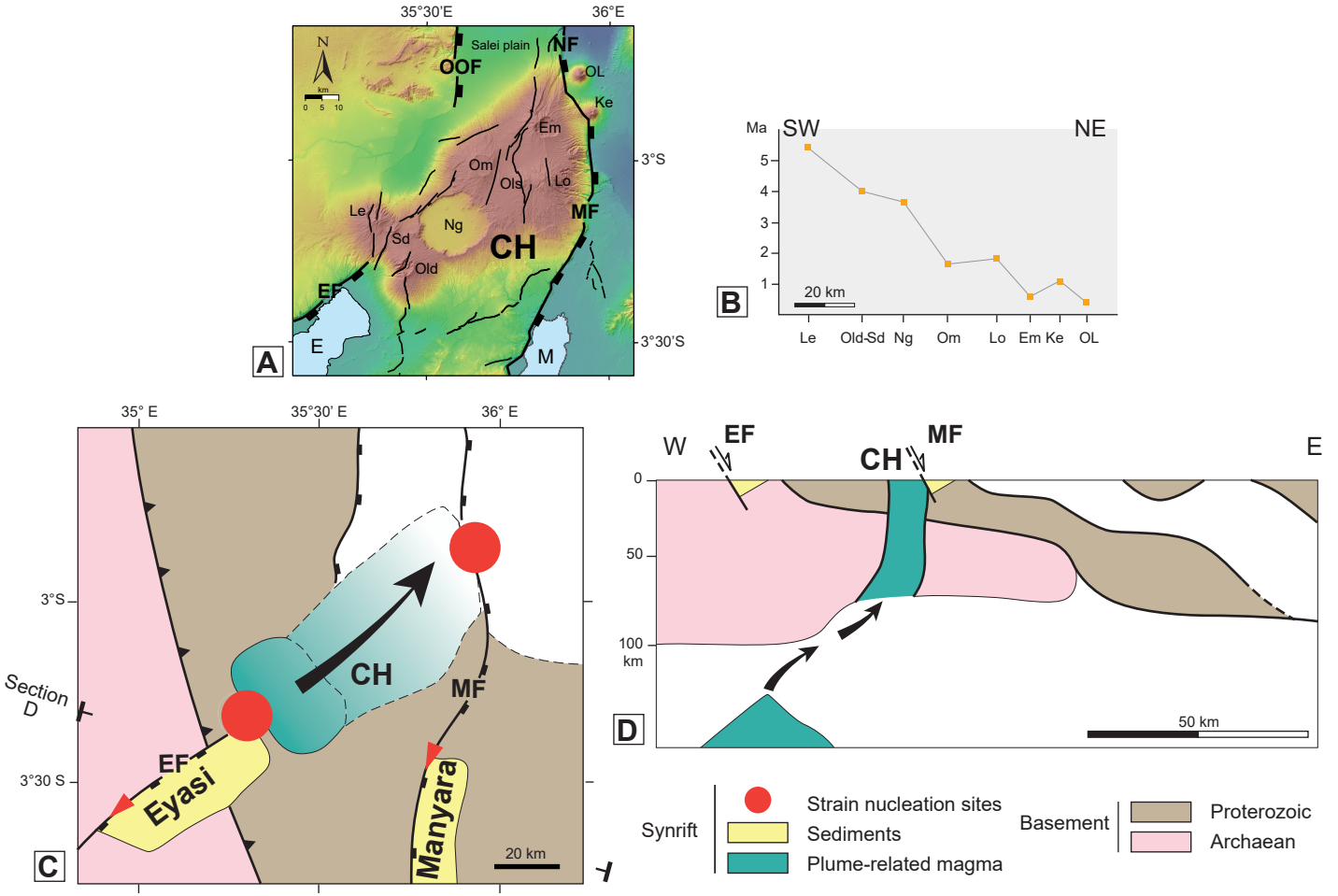

Figure 13. Strain/magmatism relationships in the western part of the NTD. A. Major tectono-magmatic structures in the Eyasi and Crater Highlands (CH) areas, extracted from the SRTM-30 DEM in Fig. 2A. Same abbreviations as in Fig. 2A. B. Diagram showing the northeasterly younging of lavas in the off-axis Crater Highlands magmatic segment. Same abbreviations as in Fig. 9. C. Sketch map showing the location of the Eyasi and Manyara strain nucleation sites at the two extremities of the Crater Highlands (CH) range. D. 2D-model showing the vertical pathway of plume-related melt/magma at the base of the step-like cratonic lithosphere (composite section based on the basement structural section in Fig. 10A).

Parameters / Section		Extension (Linear, m)					Final width (L_1, km)	Initial width (L_o, km)		Extension $(L_1-L_o)*100/L_o$(%)	
		Border Faults		Inner faults	Total						
		Min	Max		Min	Max		Min	Max	Min	Max
Magadi Segment	**A1**	5197	5772	1035	6232	6807	74	67.2	67.8	9.2	10.1
	A2	5122	5697	1147	6269	6844	71	64.2	64.7	9.7	10.7
	A3	5480	6055	788	6268	6843	72	65.2	65.7	9.5	10.5
	A4	5644	6219	947	6591	7166	69	61.8	62.4	10.6	11.6
Sonjo transfer zone	**A5**	6640	7305	765	7405	8070	77	68.9	69.6	10.7	11.7
	A6	1894	1984	827	2721	2811	73	70.2	70.3	3.9	4.0
	A7	2269	2359	814	3083	3173	69	65.8	65.9	4.7	4.8
Natron segment	**A8**	2357	2447	690	3047	3137	62	58.9	59.0	5.2	5.3
	A9	2362	2452	451	2813	2903	62	59.1	59.2	4.7	4.9
	A10	2258	2348	431	2689	2779	55	52.2	52.3	5.1	5.3
	A11	2315	2405	493	2808	2898	56	53.1	53.2	5.3	5.5
	A12	2269	2359	406	2675	2765	60	57.2	57.3	4.7	4.8
A											
Natron - OOB segment	**A8**	3094	3438	690	3784	4128	100	95.9	96.2	3.9	4.3
	A9	3615	3959	451	4066	4410	78	73.6	73.9	5.5	6.0
	A10	3298	3642	431	3729	4073	78	73.9	74.3	5.0	5.5
	A11	3292	3636	493	3785	4129	93	88.9	89.2	4.2	4.6
	A12	2997	3341	406	3403	3747	88	84.3	84.6	4.0	4.5
B											